Global Biogeochemical Cycles®

RESEARCH ARTICLE
10.1029/2021GB007178

Key Points:

- The export potential of distinct biogenic carbon pools is determined from multiple chemical and bio-optical sensors on a profiling float
- Continuous observations confirm the mechanism sustaining simultaneous particle export and heterotrophy in the Northeast Pacific
- Real-time export ratios are calculated from float-based estimates of net primary production and sinking particulate organic carbon

Supporting Information:

Supporting Information may be found in the online version of this article.

Correspondence to:

A. J. Fassbender,
andrea.j.fassbender@noaa.gov

Citation:

Huang, Y., Fassbender, A. J., Long, J. S., Johannessen, S., & Bernardi Bif, M. (2022). Partitioning the export of distinct biogenic carbon pools in the Northeast Pacific Ocean using a biogeochemical profiling float. *Global Biogeochemical Cycles*, *36*, e2021GB007178. https://doi.org/10.1029/2021GB007178

Received 30 AUG 2021
Accepted 3 JAN 2022

Partitioning the Export of Distinct Biogenic Carbon Pools in the Northeast Pacific Ocean Using a Biogeochemical Profiling Float

Yibin Huang[1,2], Andrea J. Fassbender[1,2,3], Jacqueline S. Long[3], Sophia Johannessen[4], and Mariana Bernardi Bif[3]

[1]Department of Ocean Sciences, University of California, Santa Cruz, CA, USA, [2]NOAA/OAR Pacific Marine Environmental Laboratory, Seattle, WA, USA, [3]Monterey Bay Aquarium Research Institute, Moss Landing, CA, USA, [4]Institute of Ocean Sciences, Sidney, BC, Canada

Abstract We leverage observations from chemical and bio-optical sensors mounted on a biogeochemical profiling float in the Northeast Pacific Ocean to quantify the cycling and export potential of distinct biogenic carbon pools, including particulate inorganic carbon (PIC), particulate organic carbon (POC), and dissolved organic carbon (DOC). Year-round observations reveal complex carbon cycle dynamics among these carbon pools. Net DOC production peaked during bloom initiation, about 3 months prior to the summer peak in POC production. We validate the float estimates of DOC cycling with seasonal accumulation and removal rates derived from ship-board DOC observations over the same period. By combining chemical and bio-optical tracers of POC cycling, we estimate the instantaneous POC sinking flux ($F_{POC_{sinking}}$). The cooccurrence of DOC consumption and POC production and sinking during fall and winter resolves the regional conundrum of a persistent particle sinking flux observed by sediment traps during a season that is known to be heterotrophic. PIC production is small, and uncertainties are large. By combining float-based estimates of instantaneous net primary production (NPP) and $F_{POC_{sinking}}$, we quantify a real-time carbon export ratio ($[F_{POC_{sinking}}/NPP] \times 100\%$) for the euphotic zone. Elevated export ratios during summer are associated with an increase in the fraction of particles larger than 100 μm in size. Elevated export ratios during winter are associated with the physical redistribution of particles through seasonal deep mixing. Our study demonstrates how the combined use of multiple sensors on biogeochemical profiling floats can provide more nuanced information about upper ocean carbon cycle dynamics.

1. Introduction

The transfer of organic carbon produced in the upper ocean to the deep sea, commonly referred to as the biological pump, is a critical part of the global carbon cycle that helps to regulate earth's climate (Boyd et al., 2019; Friedlingstein et al., 2020; Volk & Hoffert, 1985). Organic carbon is operationally differentiated into particulate organic carbon (POC; typically defined as particles >0.7 μm) and dissolved organic carbon (DOC; matter passing through a filter of either 0.7 or 0.22 μm). The gravitational sinking of algal cells, detritus, aggregates, and fecal matter from zooplankton grazing are thought to be the main pathways for POC export (Buesseler et al., 2020; Passow, 2002; Siegel et al., 2014). Downward mixing is thought to be the primary pathway for DOC export, accounting for approximately 20% of the total carbon export globally, but with large regional variability (Bif & Hansell, 2019; Hansell et al., 2009; Romera-Castillo et al., 2016; Roshan & DeVries, 2017). Global organic carbon export estimates range from 5 to 12 Pg C yr^{-1} (DeVries & Weber, 2017; Dunne et al., 2007; Henson et al., 2011; Laws et al., 2011; Siegel et al., 2014), while the air-to-sea transfer of carbon dioxide gas (CO_2) is presently estimated at 2.5 Pg C yr^{-1} (Friedlingstein et al., 2020; Takahashi et al., 2002). Thus, just a 10% reduction in the efficiency of the biological pump could impose a 20%–50% reduction in the ocean carbon sink.

The transfer of particulate inorganic carbon (PIC) produced in the upper ocean to the deep sea, namely the calcium carbonate counter pump, is another critical part of the global carbon cycle (Balch et al., 2007; Macreadie et al., 2017). PIC production reduces the local ocean uptake of atmospheric CO_2 while the dissolution of PIC at depth helps to buffer changes in ocean pH (Adkins et al., 2021; Feely et al., 2004). Additionally, PIC can act as ballast, augmenting the sinking rate and transfer efficiency of organic matter (Klaas & Archer, 2002). The relative contribution of each carbon pool and export pathway depends on many factors, such as phytoplankton community structure, ecosystem food webs, the strength of microbial loop, and environmental conditions. At a global scale,

the characterization of carbon pool dynamics and tighter constraint on the magnitude of the biological pump remain critical knowledge gaps. A small shift in the ratio of PIC, POC, and DOC production or export could have important implications for the depth of carbon remineralization (Carlson et al., 2010; Klaas & Archer, 2002), mesopelagic food webs (Legendre et al., 2015), the efficiency of the biological pump (Passow & Carlson, 2012), and the duration of carbon storage in the ocean (Boudreau et al., 2018; Kwon et al., 2009).

Despite the importance of this topic, the contribution of different biogenic pools to the total carbon export remains a challenge to quantify due to methodological and observational limitations. POC export is commonly estimated by measuring the $^{234}Th/^{238}U$ ratios of POC (Amiel et al., 2002; Coale & Bruland, 1985) or by using sediment traps (Buesseler, 1991; Martin et al., 1987). DOC export is almost exclusively estimated from the seasonal change in DOC inventory based on monthly or seasonally collected hydrographic data (Bif & Hansell, 2019; Carlson et al., 1994; Hansell & Carlson, 1998). PIC export is less commonly measured, but has been estimated using sediment traps (Timothy et al., 2013) and a combination of chemical tracer budgets (Fassbender et al., 2016; Williams et al., 2018). However, temporally and spatially limited measurements are not sufficient to capture the dynamic and heterogeneous nature of biogenic carbon export processes.

Autonomous platforms equipped with chemical and bio-optical sensors now make it possible to quantify carbon export at more ideal temporal and spatial scales (Bushinsky & Emerson, 2015; Plant et al., 2016; Riser & Johnson, 2008; Yang et al., 2017). However, most studies to date have focused on the evolution of bulk organic matter export and only a few have attempted to differentiate carbon pools (Alkire et al., 2012; Bif & Hansell, 2019; Fassbender et al., 2016, 2017; Haskell et al., 2020; Williams et al., 2018). For example, Alkire et al. (2012) combined simultaneous measurements of oxygen (O_2), nitrate (NO_3^-), and backscatter from a biogeochemical (BGC) profiling float in the North Atlantic Ocean to isolate the export of POC and DOC over approximately 1 month during the spring bloom. Fassbender et al. (2016) and Fassbender et al. (2017) used dissolved inorganic carbon (DIC) and total alkalinity (TA) budgets based on multiple years of mooring observations to quantify the climatological total organic carbon (POC + DOC) and PIC export production at two locations in the North Pacific Ocean; an approach subsequently applied by Williams et al. (2018) to BGC floats in the Southern Ocean. Haskell et al. (2020) were the first to characterize the climatological export of all three carbon pools (PIC, POC, and DOC) using both BGC float and mooring observations in the Northeast Pacific Ocean.

In addition to a conductivity-temperature-depth sensor, BGC profiling floats are now capable of carrying sensors that measure O_2, NO_3^-, pH, and bio-optical parameters (including chlorophyll fluorescence, particle backscatter, and color dissolved organic matter); hereafter referred to as 5-sensor floats. The addition of a pH sensor makes it possible to pair pH measurements with TA estimates to calculate DIC throughout the water column. This circumvents the need of mooring pCO_2 data to calculate mixed layer DIC concentrations, as was done in Haskell et al. (2020). Here, we rely solely on water column observations from one 5-sensor BGC float deployed near Ocean Station Papa (OSP; 50°N, −145°E; Figure 1) to quantify the euphotic-zone cycling and export potential of PIC, POC, and DOC. Using both chemical and bio-optical tracers of POC cycling, we constrain the instantaneous sinking particle flux ($F_{POC_{sinking}}$) and quantify the real-time export ratio (e-ratio) by combining float estimates of net primary production (NPP) and $F_{POC_{sinking}}$ (e-ratio = [$F_{POC_{sinking}}$/NPP] × 100%).

2. Methods

2.1. Study Domain

Our study region is located near OSP (Figure 1), a well-characterized time-series site in the subarctic northeast Pacific (Freeland, 2007; Harrison, 2002). Seasonal cruises (generally during February, June, and August) extending from the Canadian west coast to OSP have occurred since 1949, providing a long-term record of physical and biochemical ocean conditions. This region is a CO_2 sink over the course of the year (Ayers & Lozier, 2012; Takahashi et al., 2002). Alleviation of seasonal light limitation during spring triggers bloom initiation, resulting in a pronounced drawdown of macronutrients (Harrison, 2002). However, the summer exhaustion of NO_3^- is generally precluded by iron limitation, rendering this a typical high-nutrient-low-chlorophyll region (Harrison, 2002; Martin & Fitzwater, 1988).

A variety of geochemical approaches have been used to estimate regional carbon export revealing a seasonal shift between autotrophy (when gross primary production exceeds community respiration) and heterotrophy (the

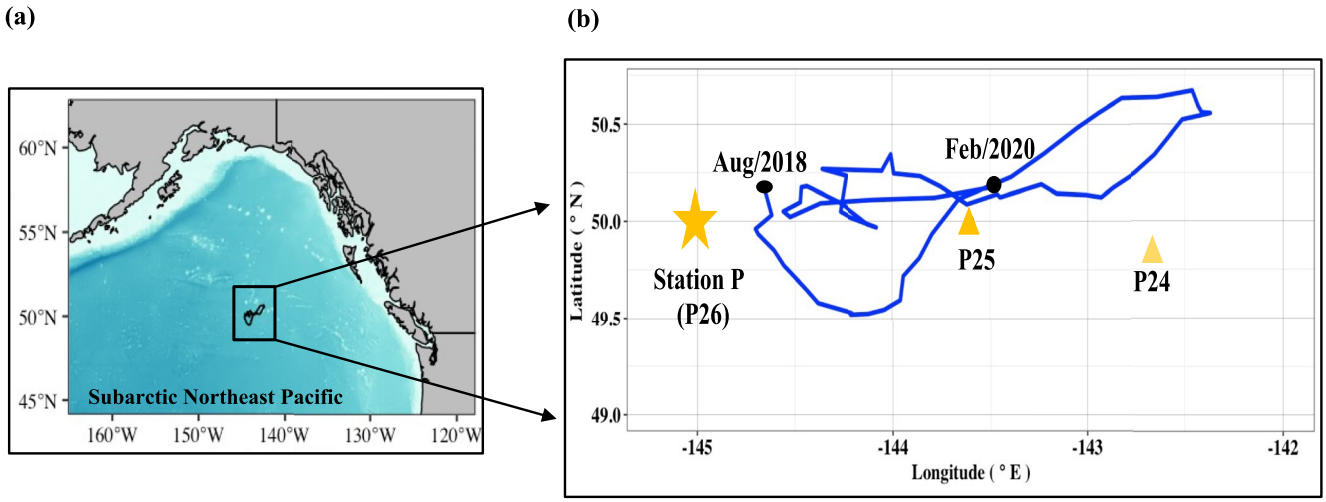

Figure 1. (left) Study domain and (right) float trajectory (line). Nearby Canadian Line P Program sampling stations (triangles), including Ocean Station Papa (OSP; star), are also shown.

opposite) with annual export hovering around 2 mol C m^{-2} yr^{-1} (Bif & Hansell, 2019; Bushinsky & Emerson, 2015; Emerson & Stump, 2010; Fassbender et al., 2016; Giesbrecht et al., 2012; Haskell et al., 2020; Timothy et al., 2013; Wong et al., 1999). Calcium carbonate ($CaCO_3$) particles are thought to play an important role in this region, accounting for up to ~30% of total carbon export (Fassbender et al., 2016; Timothy et al., 2013; Wong et al., 2002). Over the past decade, the study region has endured two marine heatwaves: from 2013 to 2015 (Bond et al., 2015) and from mid-2018 throughout early 2020 (Amaya et al., 2020; Scannell et al., 2020). Prior research on the first marine heatwave emphasized marine ecosystem impacts within the study domain caused by significant shifts in the phytoplankton community structure (Peña et al., 2018) and fish larva (Nielsen et al., 2021), as well as a decline in carbon export (Bif et al., 2019; Yang et al., 2018). Our study period is coincident with the second marine heatwave, characterized by anomalously high temperatures and low salinities (Amaya et al., 2020; Scannell et al., 2020).

2.2. Data Sources

2.2.1. Float Platform and Sensor Information

The Sea-Bird Scientific (SBS) Navis BGC float (WMO ID: 5905988) used in this study was deployed in August 2018 near OSP (Figure 1). The raw and quality-controlled float data files were retrieved from https://www.mbari.org/science/upper-ocean-systems/chemical-sensor-group/floatviz/. The float was equipped with an SBE41 conductivity-temperature-depth (CTD) sensor, SBE63 optical dissolved oxygen sensor, Satlantic Deep SUNA nitrate sensor (Johnson & Coletti, 2002), Deep-Sea DuraFET pH sensor (Johnson et al., 2016), and a WETLabs three-channel MCOMS bio-optical sensor with chlorophyll fluorescence at 470/685 nm, CDOM at 370/460 nm, and backscattering (b_{bp}) at 700 nm with a scattering angle of 150°. The float profiled every ~10 days from 2,000 m to the surface with 2 m resolution sampling in the top 200 m.

The SBE63 oxygen sensor is not capable of air calibration, so oxygen data were calibrated using the 2018 World Ocean Atlas monthly oxygen climatology. This calibration approach typically constrains float oxygen accuracy to within ±3% at the surface (Takeshita et al., 2013), which is not adequate to determine the air-sea oxygen gas flux. We re-calibrated the oxygen sensor data (i.e., values retrieved after using only the manufacturer calibration information) using high-accuracy Winker oxygen samples collected during regional Canadian Line P Program cruises to better constrain the oxygen sensor gain (Figure S1 in Supporting Information S1). This calibration approach yielded an accuracy of ~0.35%, which is comparable to the accuracy achieved by optodes capable of air calibration (Bushinsky et al., 2016). Quality control of float pH and nitrate sensor data was conducted following the standard procedures proposed by the international Biogeochemical Argo program (Johnson et al., 2017).

The quality control of b_{bp} data and partitioning of big (>100 μm in size) and small particles (<100 μm in size) followed the methods described in Briggs et al. (2020). Briefly, blank values (corresponding to mean wintertime b_{bp} values between 850 and 900 m each year) were subtracted from each b_{bp} profile before a 11-point maximum filter was applied to remove outliers caused by large particles and background noise. Small and big particles were separated by a 11-point minimum filter. b_{bp} data were converted to POC concentration using a global, empirical relationship: POC (mg m^{-3}) = 31,200 × b_{bp_700nm} (1/m) + 3.04 (Johnson et al., 2017). Raw float fluorescence data were corrected for non-photochemical quenching before a background signal (minimum Chl-*a* between 100 and 300 m) was removed. To obtain the best possible Chl-*a* estimate, fluorescence-to-chlorophyll-concentration relationships derived from Line P cruise discrete Chl-*a* samples and CTD fluorescence data were applied to the BGC float observations as described in Long et al. (2021).

Float profile data were interpolated to a 1-m vertical resolution and smoothed over time with a 5-point moving mean to filter out the short-term fluctuations. A salinity data quality issue was identified when the salinity quality control (QC) flag switched from 1 (equivalent to good data) to 4 (equivalent to bad data) in the delayed-mode file after profile 101 (March 2020) as a result of sensor drift (Bittig et al., 2019). Chemical sensor output (for O_2, pH, and NO_3^- sensors) requires salinity information to compute the chemical quantities of interest and to perform various calibration (O_2) and adjustment (pH and NO_3^-) procedures (Johnson et al., 2017; Maurer et al., 2021). As a result, the QC flags for chemical tracers were also assigned values of 4 once the salinity issue presented. Thus, our analysis was confined to the first 100 float profiles.

2.2.2. Carbonate System Calculations

TA was calculated from float temperature, salinity, and oxygen measurements using the CANYON-B neural network algorithm (Bittig et al., 2018). TA estimates were paired with float pH observations to calculate the partial pressure of CO_2 (pCO_2) and DIC using "seacarb" package in R (Gattuso et al., 2020). Near-surface pCO_2 estimates from the float show excellent agreement with preliminary pCO_2 observations from the OSP mooring (Figure S2 in Supporting Information S1). While previous studies have demonstrated the ability of CANYON-B to reproduce the magnitude and seasonal cycle of historical, ship-board TA measurements from the region (with the estimated error <1%, ±13 μmol kg^{-1}; Haskell et al., 2020), it should be noted that these empirical TA estimates integrate the influence of $CaCO_3$ processes rather than independently resolving calcification in real time. Therefore, PIC production solved from the TA budget should be interpreted with some degree of caution. DIC estimates herein are more robust due to the inclusion of float-measured pH.

2.2.3. Ancillary Data

Publicly available ancillary data used in this study include daily averages of three-hourly air pressure, 10-m wind speed, and atmospheric pCO_2 from the NOAA OSP mooring (https://www.pmel.noaa.gov/ocs/data/disdel/ and https://www.pmel.noaa.gov/co2/story/Papa/); daily euphotic zone depth (Z_{eu}, https://oceandata.sci.gsfc.nasa.gov/directaccess/MODIS-Aqua/Mapped/8-Day/9km/Zeu_lee) and surface photosynthetically active radiation (PAR; https://oceandata.sci.gsfc.nasa.gov/directaccess/MODIS-Aqua/Mapped/8-Day/9km/par/) at 0. 083° resolution; daily wind stress at 0.25° resolution from the Advanced Scatterometer product (https://manati.star.nesdis.noaa.gov/datasets/ASCATData.php); a monthly climatology of diapycnal diffusivity at the base of mixed layer from Cronin et al. (2015); seasonal discrete samples of NO_3^- and O_2 collected by the Canadian Line P Program (https://www.waterproperties.ca/linep/cruises.php); and ship-board measurements of DIC and TA collected during the August 2018 NASA EXPORTS cruise near OSP (https://seabass.gsfc.nasa.gov/experiment/EXPORTS; https://doi.org/10.5067/SeaBASS/EXPORTS/DATA001). Additional discrete samples of DIC, TA, pH, DOC, POC, and particulate organic nitrogen (PON) collected during Canadian Line P Program cruises from February 2019 through February 2020 are also used (https://www.bco-dmo.org/dataset/865829; https://doi.org/10.26008/1912/bco-dmo.865829.1; https://www.bco-dmo.org/dataset/865893; https://doi.org/10.26008/1912/bco-dmo.865893.1; https://www.ncei.noaa.gov/access/metadata/landing-page/bin/iso?id=gov.noaa.nodc:0234342). The sources and detailed usage of the ancillary data are summarized in Table S1 of Supporting Information S1. Observations from the closest (in space and time) satellite grid or Line P cruise station were matched to float profiles for calculations and parameter comparisons.

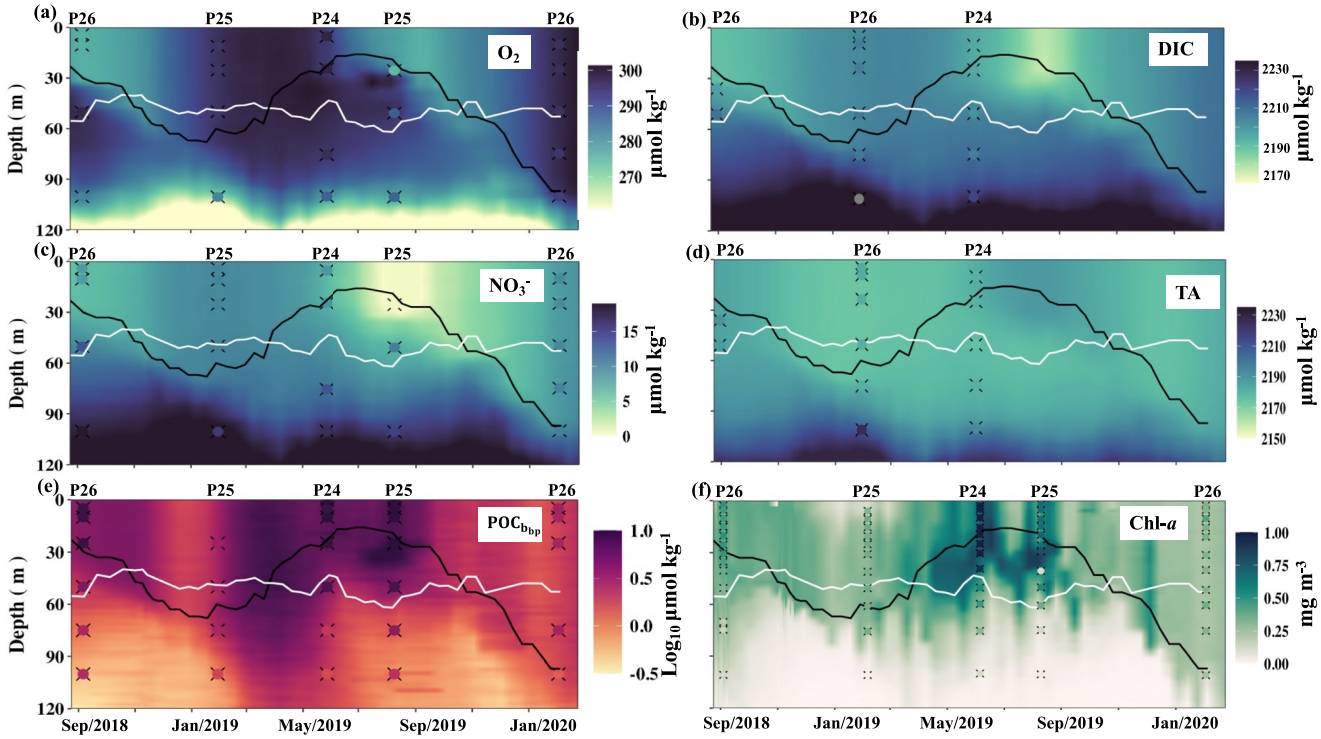

Figure 2. Time series of biogeochemical properties from float observations. Colored circles, with "×" symbols behind them, show discreet sample values from the Canadian Line P cruise station (noted above the panel) closest to the float at the time of collection. The black and white lines represent the mixed layer and euphotic zone depths, respectively.

2.3. Net Biological Metabolism Estimated From Chemical and Bio-Optical Tracer Budgets

2.3.1. Mass Balance Model

The overarching goal of our study is to characterize the cycling and export potential of distinct biogenic carbon pools using a 5-sensor BGC float and to diagnose the underlying mechanisms governing these processes. Biogeochemical tracers record the imprint of physical and biological processes in seawater. By combining O_2, NO_3^-, DIC, TA, and $POC_{b_{bp}}$ (suspended POC derived from the b_{bp} signal) observations and estimates from the float, we can close an upper-layer budget to estimate the residual, net biological metabolism in the water column over time. We focus our analysis on the euphotic zone to evaluate differences in the net production of POM, DOM, and PIC. Given the near constancy of Z_{eu} during the study period (white line in Figure 2), we closed the tracer budgets to a fixed depth of 56 m.

By assuming a negligible role of horizontal advection in this region, similar to prior studies near OSP (Bushinsky & Emerson, 2015; Emerson & Stump, 2010; Haskell et al., 2020; Yang et al., 2018), the vertically integrated time rate of change for a given tracer ($dT_{(tracer)}/dt$, mmol m^{-2} d^{-1}) can be expressed as Equation 1:

$$\frac{dT_{(\mathrm{DIC,TA,O_2,NO_3^-,POC_{b_{bp}}})}}{dt} = \frac{\partial T_{(\mathrm{DIC,O_2})}}{\partial t}\Big|_{\mathrm{Gas}} + \frac{\partial T_{(\mathrm{DIC,TA,O_2,NO_3^-,POC_{b_{bp}}})}}{\partial t}\Big|_{\mathrm{Phys}} + \frac{\partial T_{(\mathrm{DIC,TA,NO_3^-,POC_{b_{bp}}})}}{\partial t}\Big|_{\mathrm{EP}} + \frac{\partial T_{(\mathrm{DIC,TA,O_2,NO_3^-,POC_{b_{bp}}})}}{\partial t}\Big|_{\mathrm{Bio}} \quad (1)$$

The right-hand side of Equation 1 accounts for the influence of air-sea gas exchange (Gas), evaporation and precipitation (EP), physical transport and mixing (Phys), and net biological processes (Bio). The Bio term is calculated as a residual after accounting for all abiotic processes. The rationale for omitting horizontal advection in the upper layer tracer budget is supported by the weak horizontal advection of surface layer oxygen resolved from repeat Seaglider measurements near OSP (Pelland et al., 2018).

The DIC gas exchange term was calculated using Equation 2:

$$\frac{\partial \mathrm{DIC}}{\partial t}|_{\mathrm{Gas}} = k \times K_{\mathrm{H}} \times \Delta p\mathrm{CO}_2 \tag{2}$$

where k is the wind-speed dependent gas exchange velocity parameterized by Wanninkhof (2014), K_{H} is the CO_2 solubility (Weiss, 1974), and ΔpCO_2 is the difference in pCO_2 between surface seawater and the atmospheric boundary layer. Since oxygen is less soluble than CO_2, bubbles play an important role in mediating the bulk O_2 air-sea flux. As a result, many recent studies have adopted the gas model developed by Liang et al. (2013) to better constrain bubble processes in O_2 gas exchange (Bushinsky & Emerson, 2015; Pelland et al., 2018; Yang et al., 2017). This gas model explicitly incorporates the air-sea flux contributed by large bubbles that exchange gas with the water as they resurface and small bubbles that collapse and inject gas into the seawater as follows (Equation 3):

$$\frac{\partial \mathrm{O}_2}{\partial t}|_{\mathrm{Gas}} = \underbrace{K_s(\overline{\mathrm{O}_2} - \mathrm{O}_{2_{\mathrm{sat}}})}_{\text{Diffusive exchange}} + \underbrace{K_p\left\{(1+\Delta P)\mathrm{O}_{2_{\mathrm{sat}}} - \overline{\mathrm{O}_2}\right\}}_{\text{Large bubble}} + \underbrace{K_C X_{\mathrm{O}_2}}_{\text{Small bubble}} \tag{3}$$

where subscripted K values represent the gas exchange velocity for different air-sea processes (s = exchange diffusion; p = large bubble; C = small bubble); $\overline{\mathrm{O}_2}$ is the average O_2 concentration within the mixed layer; ΔP is the elevated bubble pressure; $O_{2_{\mathrm{sat}}}$ is oxygen saturation concentration calculated from temperature, salinity, and air pressure (Garcia & Gordon, 1992); X_{O_2} is the mole fraction of oxygen in air.

The physical transport and mixing terms at the base of Z_{eu} consist of diapycnal diffusion and Ekman pumping, shown here for NO_3^- (Equation 4):

$$\frac{\partial \mathrm{NO}_3^-}{\partial t}|_{\mathrm{Phys}_{Z_{eu}}} = \underbrace{K_{z\_Z_{eu}} \times \frac{\partial \mathrm{NO}_3^-}{\partial z}|_{Z_{eu}}}_{\text{Diapycnal diffusion}} + \underbrace{w_{Z_{eu}} \times (\overline{\mathrm{NO}_3^-} - \mathrm{NO}_{3_{Z_{eu}}}^-)}_{\text{Ekman pumping}} \tag{4}$$

where $K_{z\_Z_{eu}}$ is the diapycnal coefficient, $\partial \mathrm{NO}_3^-/\partial z|_{Z_{eu}}$ is the vertical nitrate gradient, $w_{Z_{eu}}$ is the Ekman pumping velocity derived from wind stress fields following Signorini et al. (2001), and $\mathrm{NO}_{3_{Z_{eu}}}^-$ is the nitrate concentration, all evaluated at the base of the euphotic layer. $\overline{\mathrm{NO}_3^-}$ is the averaged nitrate concentration within the euphotic zone. At OSP, Kz at the base of the mixed layer (MLD) is well constrained by prior heat and salt budget calculations (Cronin et al., 2015) and microstructure measurements from Sun et al. (2013) that suggest an exponential decay in K_z beyond the base of the MLD to its background value (10^{-5} m^2 s^{-1}) over a 20 m length scale. The depth of the MLD was determined as a density increase of 0.03 relative to the 10 m density (de Boyer Montégut et al., 2004). To estimate Kz at the base of the euphotic zone, we scaled climatological Kz values at the base of the MLD using a 1/e scaling (Bushinsky & Emerson, 2015; Yang et al., 2018). This approach only works when the euphotic depth is deeper than the MLD. When the euphotic depth is shallower than the MLD, the physical transport and mixing terms computed for the full MLD are scaled as follows (Equation 5):

$$Z_{eu} < \mathrm{MLD}: \quad \frac{\partial \mathrm{NO}_3^-}{\partial t}|_{\mathrm{Phys}_{Z_{eu}}} = \frac{\partial \mathrm{NO}_3^-}{\partial t}|_{\mathrm{Phys}_{\mathrm{MLD}}} \times \frac{Z_{eu}}{\mathrm{MLD}} \tag{5}$$

This approach assumes that the impacts of physical transport and mixing occurring at the base of the MLD will be equally distributed throughout the mixed water column and requires that entrainment or detrainment be considered (Equation 6):

$$\frac{\partial \mathrm{NO}_3^-}{\partial t}|_{\mathrm{Phys}_{\mathrm{MLD}}} = \underbrace{K_{Z_{\mathrm{MLD}}} \times \frac{\partial \mathrm{NO}_3^-}{\partial z}|_{\mathrm{MLD}}}_{\text{Diapycnal diffusion}} + \underbrace{w_{\mathrm{MLD}} \times (\overline{\mathrm{NO}_3^-} - \mathrm{NO}_{3_{\mathrm{MLD}}}^-)}_{\text{Ekman pumping}} + \underbrace{\frac{d\mathrm{MLD}}{dt} \times (\overline{\mathrm{NO}_3^-} - \mathrm{NO}_{3_{\mathrm{MLD}}}^-)}_{\text{Entrainment/Detrainment}} \tag{6}$$

where dMLD/dt is the MLD time rate of change.

The EP term for each tracer was estimated by using the ratio of the tracer to salinity at the start of the study period ($t1$) and multiplying by the net EP salinity changes based on the salinity budget ($\partial \mathrm{Sal}/\partial t|_{\mathrm{EP}}$, Equation 7), following Fassbender et al. (2016):

$$\frac{\partial T_{(\mathrm{DIC,TA,NO_3^-,POC_{b_{bp}}})}}{\partial t}|_{\mathrm{EP}} = \frac{\partial \mathrm{Sal}}{\partial t}|_{\mathrm{EP}} \times \frac{T_{(\mathrm{DIC,TA,NO_3^-,POC_{b_{bp}}})}}{\mathrm{Sal}}|_{t1} \quad (7)$$

$\partial \mathrm{Sal}\ /\partial t|_{\mathrm{EP}}$ is computed as the difference between observed salinity changes and estimates of the physical term (Equation 8, Figure S3 in Supporting Information S1):

$$\frac{\partial \mathrm{Sal}}{\partial t}|_{\mathrm{EP}} = \frac{\mathrm{dSal}}{\mathrm{dt}} - \frac{\partial \mathrm{Sal}}{\partial t}|_{\mathrm{Phys}} \quad (8)$$

Having accounted for all abiotic processes, the net biological term can be quantified as the residual. When integrated over different depth horizons, the biological term has different meanings. Mixed layer integrations provide information about how biological processes drive air-sea gas fluxes (Körtzinger et al., 2008). Integrating to the deepest winter ventilation depth provides an estimate of carbon that is exported from the upper layer by fully accounting for the productivity below the MLD during summer as well as the entrainment of remineralized carbon during winter mixing (Palevsky & Doney, 2018). The euphotic zone integration sets an upper limit on the organic matter available for export to depth (i.e., the export potential) and reflects the overall balance of autotrophic and heterotrophic processes in the sunlit ocean.

2.3.2. Partitioning Export Potential Into Distinct Biogenic Pools

The net biological terms estimated from DIC and TA budgets encompass the production of total organic matter (TOM = POM + DOM) and PIC, whereas net biological terms estimated from NO_3^- and O_2 budgets include only TOM production (Equation 9):

$$\mathrm{Bulk\ production} = \overbrace{\underbrace{\mathrm{POM + DOM}}_{\frac{\partial T_{(\mathrm{DIC,TA})}}{\partial t}|_{\mathrm{Bio}}} + \mathrm{PIC}}^{\frac{\partial T_{(\mathrm{NO_3^-,O_2})}}{\partial t}|_{\mathrm{Bio}}} \quad (9)$$

The biological terms in the DIC and TA budgets can be broken down into the TOM and PIC components using the DIC:TA: ratios of 1:2 for calcification and −117:17 for TOM production (Anderson & Sarmiento, 1994), following Fassbender et al. (2016) (Equations 10 and 11):

$$\frac{\partial \mathrm{DIC}}{\partial t}|_{\mathrm{TOM}} = \frac{\frac{\partial \mathrm{TA}}{\partial t}|_{\mathrm{Bio}} - \left(\frac{1}{\mathrm{DIC:TA_{PIC}}} \times \frac{\partial \mathrm{DIC}}{\partial t}|_{\mathrm{Bio}}\right)}{\left(\frac{1}{\mathrm{DIC:TA_{TOM}}} - \frac{1}{\mathrm{DIC:TA_{PIC}}}\right)} \quad (10)$$

$$\frac{\partial \mathrm{DIC}}{\partial t}|_{\mathrm{PIC}} = \frac{\partial \mathrm{DIC}}{\partial t}|_{\mathrm{Bio}} - \frac{\partial \mathrm{DIC}}{\partial t}|_{\mathrm{TOM}} \quad (11)$$

After isolating the PIC term, we have four independent estimates of the TOM term from the DIC, TA, NO_3^-, and O_2 budgets. In principle, the DOM and POM portions of TOM can be partitioned by using two of the TOM terms with their corresponding stoichiometric ratios for dissolved and particulate organic matter. Given the more consistent time-integrated signals and error sources in the biological terms estimated from DIC and NO_3^- (see Section 3.2), we used the DIC and NO_3^- budget biological terms to isolate POM and DOM components following Haskell et al. (2020) (Equations 12 and 13):

$$\frac{\partial \mathrm{DIC}}{\partial t}|_{\mathrm{DOM}} = \frac{\frac{\partial \mathrm{NO_3^-}}{\partial t}|_{\mathrm{Bio}} - \left(\frac{1}{\mathrm{C:N_{POM}}} \times \frac{\partial \mathrm{DIC}}{\partial t}|_{\mathrm{TOM}}\right)}{\frac{1}{\mathrm{C:N_{DOM}}} - \frac{1}{\mathrm{C:N_{POM}}}} \quad (12)$$

$$\frac{\partial \mathrm{DIC}}{\partial t}|_{\mathrm{POM}} = \frac{\partial \mathrm{DIC}}{\partial t}|_{\mathrm{TOM}} - \frac{\partial \mathrm{DIC}}{\partial t}|_{\mathrm{DOM}} \quad (13)$$

where $\mathrm{C:N_{POM}}$ and $\mathrm{C:N_{DOM}}$ represent the end-member nutrient ratios for particulate and dissolved organic matter, respectively.

We use a $C:N_{DOM}$ ratio of 14 ± 1 based on the seasonal DOC and dissolved organic nitrogen inventory changes in our study region (Bif & Hansell, 2019) and a $C:N_{POM}$ ratio of 5.5 ± 1 based on the mean C:N ratio of suspended particles within the euphotic zone derived from the three Canadian Line P cruises occupied in August 2018, February 2019, and June 2019. A $C:N_{POM}$ of 6.6 ± 1 was applied in Haskell et al. (2020), which was calculated by averaging the C:N ratio for suspended particles (~5.5) and sinking particles (~8.8; Timothy et al., 2013; Wong et al., 1999), which were collected by sediment traps at 100–200 m depth. A higher C:N ratio in sinking particles is caused by the preferential remineralization of nitrogen over carbon by heterotrophs (Wong et al., 2002).

Ship-based DOC observations were averaged across three Line P stations (P24, P25, and P26) near the float trajectory path for each cruise (Figure 1). The coarse temporal (seasonal) and vertical (~25 m) resolution of shipboard DOC measurements made it difficult to parameterize the role of physical mixing on the DOC inventory. Therefore, seasonal changes in the average euphotic zone DOC inventory provide only a first-order constraint in the float DOC production estimate. With this constraint, we find that a $C:N_{POM}$ of 6.6 cannot reproduce the DOC production observed during summer 2020 (Figure S4 in Supporting Information S1 and Section 3.3.2). Since suspended particles in the euphotic zone mainly consists of living organisms (and a small fraction of detrital components), the C:N ratio of suspended particles (5.5 ± 1) likely provides a more realistic constraint on the $C:N_{POM}$ for newly produced particles. Other processes, including N_2 fixation (Wang et al., 2019), denitrification (Tyrrell & Lucas, 2002), anthropogenic carbon accumulation (Sabine & Tanhua, 2010), and ocean mixing (Carter et al., 2021) can also alter C:N ratios inferred from the tracer budget. However, there is no evidence that these processes contribute significantly at the study site (Deutsch et al., 2001; Harrison, 2002; Tang et al., 2019) or over the duration of our 2019 analysis. Good agreement between float estimates of DOC production and ship-board measurements of seasonal DOC accumulation and removal rates (see Section 3.3.2 and Figure 6) supports our choice of endmember C:N ratios.

Solving the DIC tracer budget for POM production ($\partial DIC/\partial t|_{POM}$) yields the chemical signature of net POM production. These particles could be accumulating within the euphotic zone, sinking through the water column, or a combination of both processes. Therefore, this term can only be interpreted as particle export when integrated over a sufficient time scale, which is generally 1 year. The net biological term in the bio-optical, POC tracer budgets ($\partial POC_{b_{bp}}/\partial t|_{Bio}$) reflects the near real-time change in euphotic zone particle inventory and is equivalent to the total net POC production minus the loss of POC via gravitational sinking (Alkire et al., 2012). By combining the DIC and $POC_{b_{bp}}$ tracer budget terms, we can compute the export of sinking particles (Equation 14):

$$F_{POC_{sinking}} = \frac{\partial DIC}{\partial t}|_{POM} - \frac{\partial POC_{b_{bp}}}{\partial t}|_{Bio} \quad (14)$$

2.3.3. Error Estimates

A Monte Carlo approach was used to propagate and quantify uncertainty in the tracer budgets. Multiple sources of error (including sensor uncertainty, parameterizations of abiotic processes, end-member nutrient ratios, and mixed layer and euphotic zone depth criteria) were considered. Randomly distributed errors for each budget term were generated according to the error assignments presented in Table 1 and 10,000 simulations in which these errors were varied within their standard deviations.

2.4. Net Primary Production and Export Ratio Estimates

Estimates of in situ NPP were computed by applying the Carbon-based Productivity Model (CbPM; Westberry et al., 2008; Behrenfeld et al., 2005) to simultaneous satellite observations (PAR) and depth-resolved float observations (b_{bp}, Chl-*a*) that have been rigorously calibrated against Canadian Line P Cruise observations (Long et al., 2021). Briefly, NPP is a product of phytoplankton carbon biomass ($C_{phytoplankon}$) and growth rate (μ), the former corresponding to POC concentration computed from the float b_{bp} observations and the latter being an empirical function of b_{bp}, Chl-*a* (from float observations), and PAR (from satellite observations, Equation 15):

$$NPP = C_{phytoplankton}(b_{bp}) \times \mu(b_{bp}, Chla, PAR) \quad (15)$$

The carbon export ratio (*e*-ratio) was calculated as $F_{POC_{sinking}}$ divided by NPP (Equation 16):

$$e\text{-ratio} = \frac{F_{POC_{sinking}}}{NPP} \times 100\% \quad (16)$$

Table 1
Summary of Errors Used in the Monte Carlo Calculations

Sources	Error	Reference
O_2 measurement	±0.5%	Bushinsky et al. (2016)
pH measurement	±0.005	Johnson et al. (2016)
NO_3^- measurement	±0.5 μmol kg^{-1}	Johnson and Coletti (2002)
TA estimates	±13 μmol kg^{-1}	Bittig et al. (2018)
$POC_{b_{bp}}$ estimates	±30%	Graff et al. (2015)
CO_2 gas model	±30%	Bender et al. (2011) and Wanninkhof (2014)
O_2 gas model	±10% for Ks and ±30% for Kc and Kp	Emerson et al. (2019)
Eddy diffusivity coefficient	±30%	Cronin et al. (2015)
Ekman pumping velocity	±50%	Haskell et al. (2020)
Thickness of MLD	±0.5 m	Vertical resolution/4
Thickness of euphotic zone	±5 m	Seasonal deviation from annual mean
C:N ratio for POM/DOM production	±1	Haskell et al. (2020)

Note. NO_3^-, nitrate; TA, total alkalinity; Ks, gas exchange velocity for O_2 at the air-sea interface; Kc, gas exchange velocity for the large O_2 bubble; Kp, gas exchange velocity for the small O_2 bubble; MLD, mixed layer depth; $POC_{b_{bp}}$, particulate organic carbon estimated from the backscatter signal; POM, particulate organic matter; DOM, dissolved organic matter.

3. Results and Discussion

3.1. Seasonal Tracer Evolution

O_2, DIC, NO_3^-, TA, $POC_{b_{bp}}$, and Chl-*a* displayed pronounced seasonality within the euphotic zone (Figure 2) with the temporal evolution of the inventory integrated over the upper 56 m shown in Figure S5 of Supporting Information S1. The float observations and estimates agree well with near-contemporaneous ship-board observations that occurred in the vicinity of the float profile (Figure 2 and Figures S6–S8 in Supporting Information S1); however, these comparisons are somewhat confounded by spatiotemporal mismatches. The mechanisms governing seasonal tracer changes within the euphotic zone were revealed by closing the biogeochemical tracer budgets (Figure 3). The drawdown of DIC and NO_3^- during spring and summer was caused by biological productivity, whereas the elevation of DIC and NO_3^- during fall and winter was caused by the combined effect of physical mixing and net heterotrophic activity (Figures 3b and 3c). Gas exchange resulted in the net transfer of CO_2 from the atmosphere to the ocean at a relatively low but constant rate that contributed significantly to the annual DIC budget (Figure S9 in Supporting Information S1). Biological activity and physical transport are the primary processes influencing the TA budget (Figure 3d). The production of organic matter causes TA to increase (Brewer & Goldman, 1976) such that the observed seasonal pattern of TA has the opposite phase to that of DIC and NO_3^-. The study region is typically characterized with net precipitation over the annual cycle (Fassbender et al., 2016; Timothy et al., 2013); however, evaporation and precipitation term was insignificant during our study period. O_2 showed a seasonal pattern with a higher values in the winter and a lower value in the summer (Figure 3a), following expectations associated with temperature-induced solubility changes (Garcia & Gordon, 1992). The summer decline in O_2 was a result of O_2 gas exchange efflux outpacing the rate of biological O_2 generation. During early spring, we observed an increase in the $POC_{b_{bp}}$ inventory dominated by biological processes (Figure 3e). During fall and winter, the $POC_{b_{bp}}$ inventory was mediated by biological consumption and physical transport out of the euphotic zone.

3.2. Net Biological Production Estimated From Multiple Tracers

The multiple sensors on the BGC float provided a unique opportunity to compare the net biological terms estimated from different tracers. To facilitate comparisons, organic matter stoichiometries were used to convert NO_3^-, O_2, and TA terms to carbon units (Figure 4a). Among the four chemical tracers, DIC, TA, and NO_3^- showed the best synchronicity of elevated production during July and depressed production, including occasional heterotrophy, during winter, consistent with previously reported seasonal patterns (Bushinsky & Emerson, 2015;

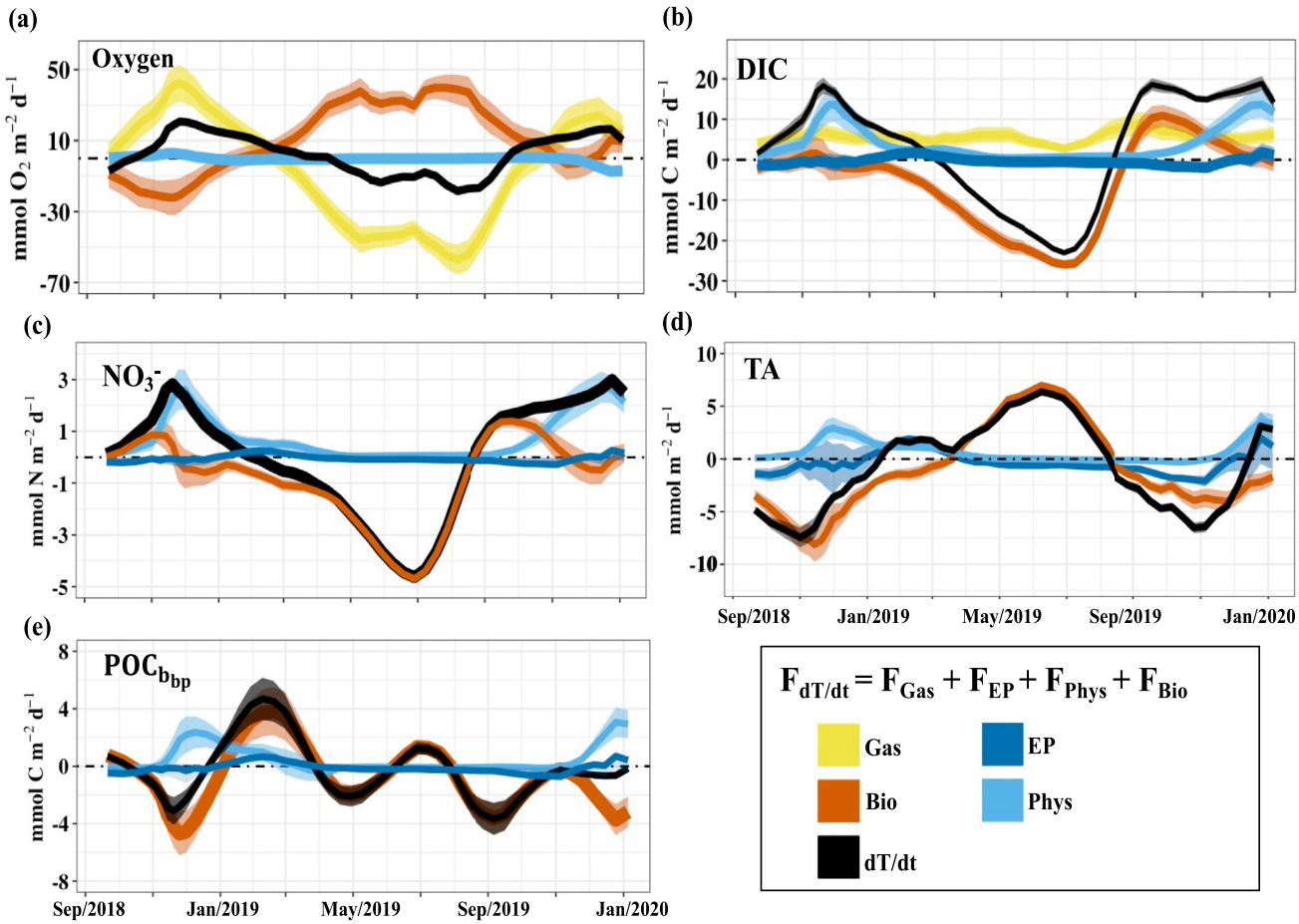

Figure 3. The temporal evolution of processes acting on biogeochemical tracers (T) in the euphotic zone. Positive values represent fluxes that cause an increase in the tracer inventory. Shading represents the uncertainty associated with each term. The evaporation and precipitation (EP) term was multiplied by 50 to improve visibility in the NO_3^- budget panel. Notably, the biological production of organic matter results in the consumption of DIC and NO_3^- but the generation of O_2, TA, and POC, while calcification results in the consumption of DIC and TA. *dT*/*dt*, time rate of change of the tracer; Gas, air-sea gas exchange; Phys, physical transport and mixing; Bio, biological process.

Fassbender et al., 2016; Plant et al., 2016). The 2019 annual net organic carbon production estimates from these tracers (DIC budget: 2.7 ± 0.6 mol C m^{-2} yr^{-1}; TA budget: 2.5 ± 0.8 mol C m^{-2} yr^{-1}; NO_3^- budget: 2.6 ± 0.6 mol C m^{-2} yr^{-1}; Figure S9 in Supporting Information S1) also fall within the bounds of prior estimates that range from 1-3 mol C m^{-2} yr^{-1}. The 2019 annual net organic carbon production derived from O_2 (4.5 ± 1.5 mol C m^{-2} yr^{-1}; C:O = 1.45) is nearly double the estimates from other tracers (Figure S9 in Supporting Information S1). Possible reasons for this discrepancy are discussed below.

The biological term estimated from $POC_{b_{bp}}$ reflects the near real-time change in POC inventory, which is a balance between the total net POC production and POC removal by gravitational sinking (Alkire et al., 2012). Weak seasonality in $POC_{b_{bp}}|_{Bio}$ relative to chemical tracer budget biological terms (Figure 4a) implies that the majority of newly produced POC is rapidly exported from, rather than accumulated within, the euphotic zone. Such efficient particle export via sinking aligns with the high sinking rates for particles (100–350 m d^{-1}) previously inferred from sediment trap measurements in the study region (Timothy et al., 2013).

A key assumption in our methodology for partitioning biogenic carbon pools is that biological budget terms reflect processes that are related through well-known stoichiometries. In practice, a variety of factors can interfere with the decomposition, including uncaptured processes, errors in the biological term estimates, variability in organic matter stoichiometries, and different timescales captured by the tracers based on their residence times. Since the biological term is solved as a budget residual, its uncertainty is largely dependent on how accurately the abiotic processes can be estimated. Physical transport (primarily through diapycnal diffusion) is the dominant

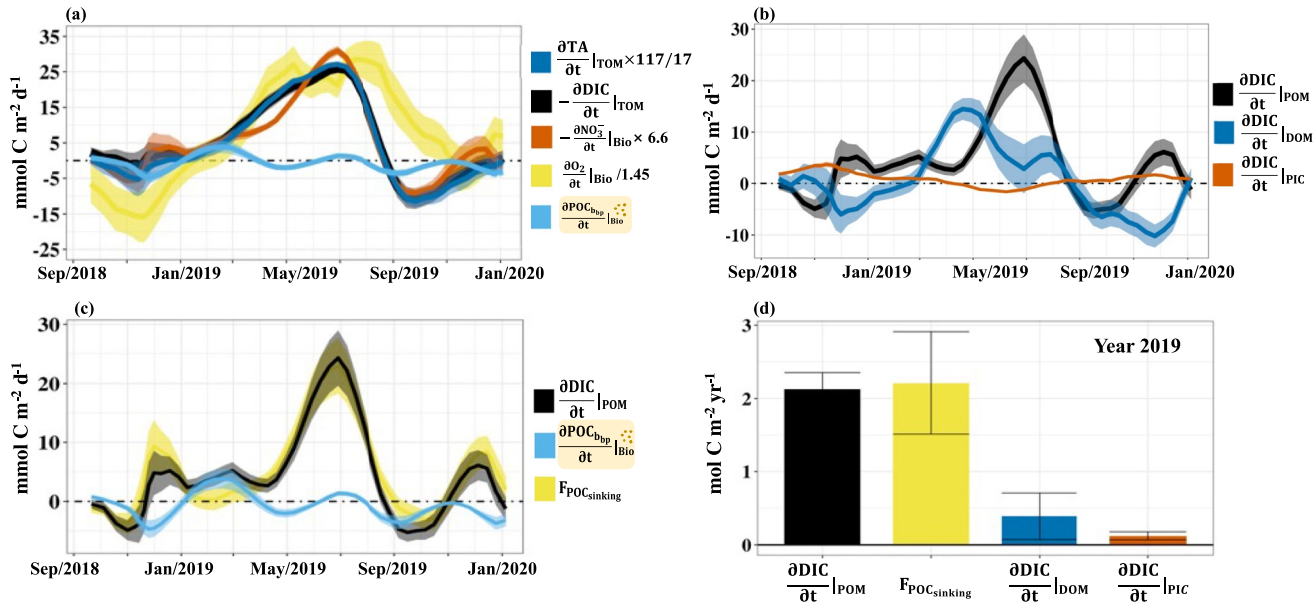

Figure 4. (a) Net biological terms estimated from the chemical and bio-optical tracer budgets, (b) partitioning of distinct biogenic carbon pools, (c) POC fluxes, including the in situ sinking flux determined by combining chemical and bio-optical tracer budgets, and (d) the annually integrated euphotic zone export potential of distinct biogenic carbon pools for the year 2019. For comparison, O_2, NO_3^-, and TA-based fluxes were converted to carbon units using organic matter stoichiometries. Shading in panels (a–c) and black lines in panel (d) represent uncertainties.

abiotic process in the DIC, TA, and NO_3^- budgets. The climatological diapycnal diffusion in our study region was previously quantified by Cronin et al. (2015) using Station Papa mooring data to close mixed layer heat and salt budgets. Elevated diapycnal diffusion of NO_3^-, TA, and DIC during the fall and winter (Figure 3) is primarily caused by stronger winds, rapid heat loss, and more frequent storms that reduce water column stability and enhance the vertical mixing, resulting in 3–10 times higher diapycnal coefficients than those in summer (Alford et al., 2012; Cronin et al., 2015). However, wintertime diapycnal coefficient estimates have considerable uncertainty due to the existence of an isothermal "barrier" layer below the mixed layer that prevents diffusive mixing and makes it challenging to estimate the diapycnal coefficient (Cronin et al., 2015). Recent studies have shown promise in measuring diapycnal diffusivity in situ by attaching a microstructure profiler to Argo floats (Roemmich et al., 2019; Shroyer et al., 2016). We anticipate that future extensions of such work to BGC floats would help to further refine physical transport terms and reduce tracer budget uncertainties.

Gas exchange is paramount among the abiotic processes in the O_2 budget (Figure 3b). In our study region, prior efforts have been made to optimize the gas model for air-sea O_2 exchange. For example, Plant et al. (2016) used $\partial NO_3^-/\partial t|_{Bio}$ estimates to tune existing O_2 gas models and force $\partial O_2/\partial t|_{Bio}$ to reproduce the seasonal $\partial NO_3^-/\partial t_{Bio}$ results (using the Redfield ratio for NO_3^-:O_2 conversion). However, it is worth noting that Plant et al. (2016) used a constant, low diffusivity coefficient (10^{-5} m^{-2} s^{-1}) to parameterize diapycnal diffusion, which likely underestimates winter mixing and may bias $\partial NO_3^-/\partial t|_{Bio}$ low. This could cause the gas models to be incorrectly tuned. More recently, Emerson et al. (2019) used in situ measurements of N_2 gas at OSP to revise the bubble term in the gas model of Liang et al. (2013). To explore whether using different gas parameterizations can narrow the gap between O_2 and the other three chemical tracer biological terms, we recomputed $\partial O_2/\partial t|_{Bio}$ using multiple gas exchange parameterizations (Figure S10a in Supporting Information S1). The annual organic carbon production derived from the multiple O_2 gas models varied between 2.1 and 4.5 mol C m^{-2} yr^{-1} but none were able to reproduce the temporal pattern of $\partial NO_3^-/\partial t|_{Bio}$ and $\partial DIC/\partial t|_{Bio}$ (Figure S10b in Supporting Information S1).

The shorter residence time of oxygen relative to the other chemical tracers may also be a source of discrepancy in the residual biological terms. The estimated residence time for O_2 in our study is on the order of a few weeks to a month, whereas the residence time for DIC with respect to air-sea gas exchange spans several months to 1 year (Figure S11 in Supporting Information S1). The relatively short O_2 residence time means that this tracer can only record very recent biologically induced saturation anomalies before they are eroded by air-sea exchange. In

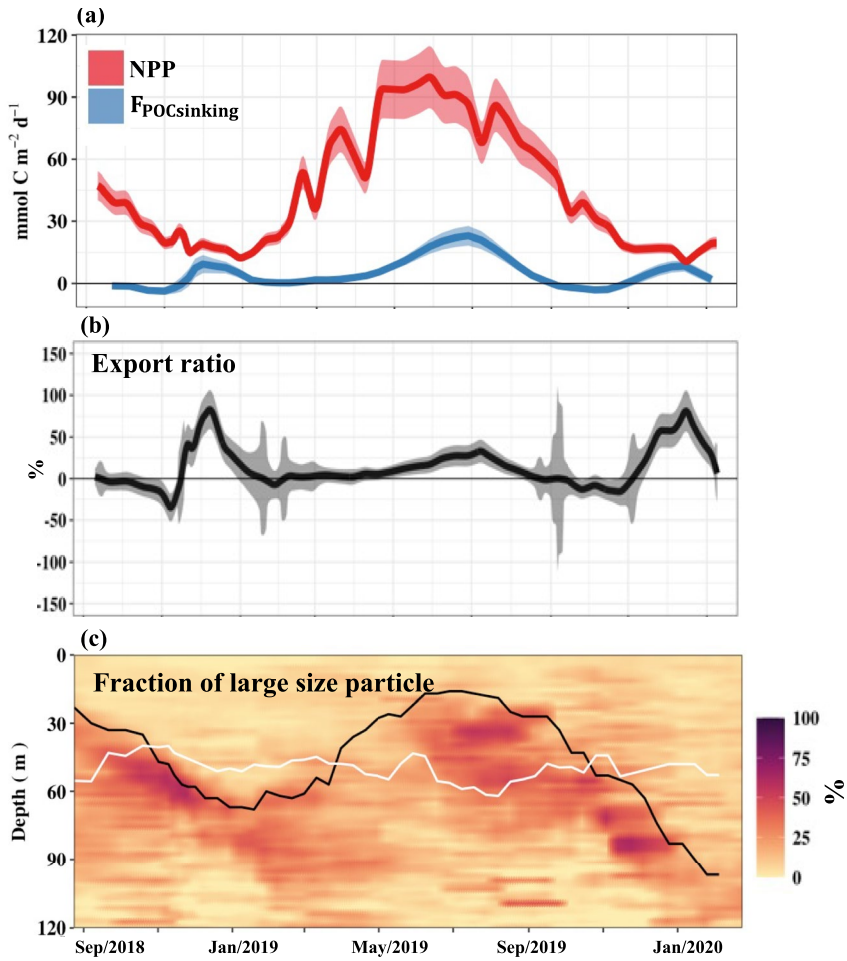

Figure 5. Temporal evolution of (a) sinking POC flux ($F_{POC_{sinking}}$) and net primary production (NPP), (b) the carbon export ratio ($F_{POC_{sinking}}$/NPP × 100%), and (c) the fraction of large (>100 μm) particles. The shading in panels (a and b) represents uncertainty. The black and white lines in panel (c) represent the mixed layer and euphotic zone depths, respectively.

summer and early fall, the residence time of O_2 is often less than the float profiling frequency (~10 days; Figure S11a in Supporting Information S1), which means that episodic, biologically induced oxygen signals may not be observed. This helps to explain the more pronounced discrepancy in net biological terms between O_2 and the other tracer estimates during this time of the year. In contrast, the mechanism that erodes biologically generated signals in DIC, TA, and NO_3^- is vertical mixing or horizontal advection, which generally occurs seasonally (Chou et al., 2005; Quay & Stutsman, 2003; Wong et al., 1999). Therefore, estimates of the net biological term based on DIC, TA, and NO_3^- tracers reflect a more consistent, accumulated biological signal. This is the primary reason we use DIC and NO_3^- to partition the biological term into distinct carbon pools.

3.3. Export Potential of Distinct Biogenic Carbon Pools

3.3.1. Seasonal Dynamics

The year-round partitioning of distinct biogenic carbon pools revealed complex carbon cycle dynamics (Figures 4b and 4c). Bloom initiation occurred in spring as reflected by the gradual increase in Chl-*a* and NPP (Figures 2f and 5a). DOC production increased with bloom development and reached a peak in May, coincident with the peak in NPP. The synchronicity between DOC production and NPP implies that changes in DOC production during this period are likely associated with the phytoplankton release of DOC during photosynthesis (Regaudie-de-Gioux et al., 2014; Myklestad, 2000; Teira et al., 2001). With a progressive increase in light availability, the bloom continued to develop into the summer with sustained NPP, high POC production, high POC sinking

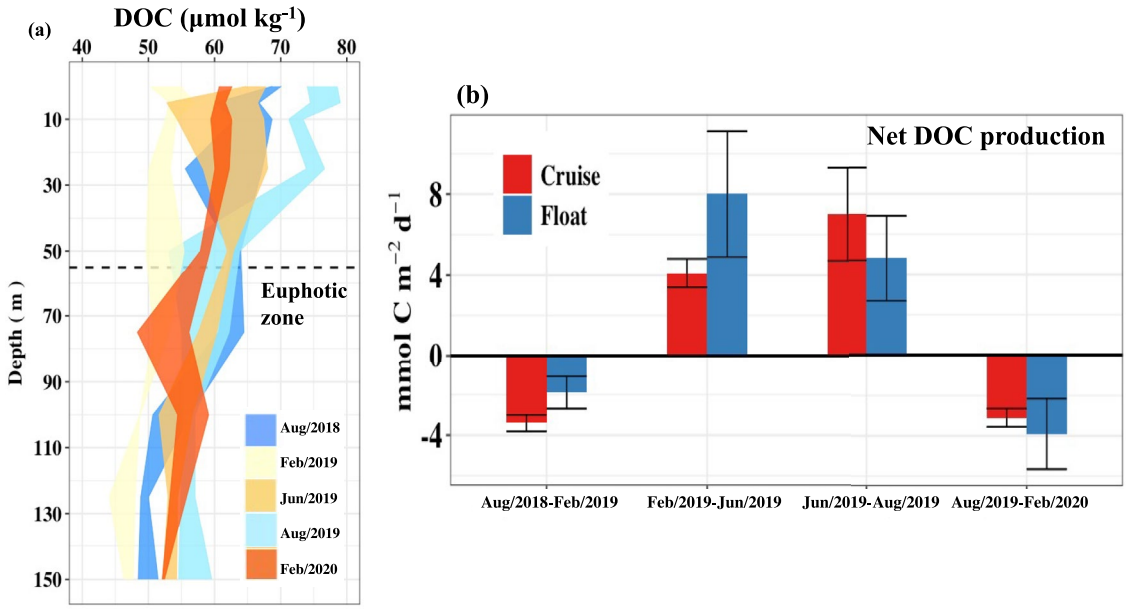

Figure 6. (a) Vertical profiles of dissolved organic carbon (DOC) collected during five Line P cruises. The shading for each profile represents the average concentration across three neighboring stations (P24, P25, and P26) and the associated standard deviation. (b) Comparison of seasonal DOC production estimates from float and ship-board observations in the upper 56 m.

flux, and slightly negative PIC production (Figure 4b). Negative PIC production suggests dissolution of $CaCO_3$ within the euphotic zone. This is unexpected because the saturation horizons for aragonite (~300 m) and calcite (~700 m) are much deeper than the euphotic zone in our study region (Feely et al., 2004; Sulpis et al., 2021). However, late spring through summer often coincides with vigorous bacterial and zooplankton activity (Goldblatt et al., 1999; Landry et al., 1993; Sherry et al., 1999, 2002), which could mean that $CaCO_3$ dissolution was occurring in acidic microenvironments within particles and aggregates or within zooplankton guts (Carter et al., 2021; Sulpis et al., 2021).

The vigorous summertime POC sinking flux aligns with historical sediment trap records from the region that shows a summer maximum in particle flux (Timothy et al., 2013; Wong et al., 1999). Combining the export flux with the contemporaneous float estimate of NPP, a high summertime export ratio (30 ± 15%, mean ± error) was observed (Figures 5a and 5b). During this period, the backscatter sensor revealed an increasing fraction of large particles (>100 μm) above the Z_{eu} (Figure 5c). This may suggest a shift in the phytoplankton community (Harrison, 2002; Peña et al., 2018) that led to faster sinking rates and elevated export efficiency. Alternatively, the gradual decline in NPP over this period could suggest that the increase in large particles may be attributed to an increase in zooplankton abundance (Haentjens et al., 2020; Lacour et al., 2019). The top-down control exerted by zooplankton grazing would lower NPP but also facilitate the formation of dense fecal pellets and aggregates with faster sinking rates, giving rise to the higher carbon export efficiency (Cavan et al., 2017).

Elevated large particle fractions were found to occur at depths in the water column that covary with the MLD throughout the year (Figure 5c). Such synchrony implies that the summer increase in large particle fraction within the Z_{eu} may be induced by a passive, physically mediated isopycnal uplift of the community (Ma et al., 2020) or active vertical migration of the community in response to the changing environmental conditions (i.e., light, nutrient availability, and buoyancy). DOC production in summer was lower than that in spring, which is likely related to enhanced DOC consumption by the microbial loop since peak bacterial abundance and production in this region generally occur during summer (Sherry et al., 1999, 2002). As the bloom subsided into the fall (reflected by a significant reduction in NPP), DOC exhibited a late August maxima (Figure 4b) possibly caused by excretion or phytoplankton cell lysis during zooplankton grazing (Hygum et al., 1997; Lampert, 1978).

A lingering puzzle in this study region is the persistent flux of particles year round, as observed by sediment traps (Timothy et al., 2013), in conjunction with oscillating autotrophic and heterotrophic seasons. In order to exhibit heterotrophy while carbon export is occurring, Fassbender et al. (2016) posited that heterotrophy is caused by

the respiration of previously produced DOC outcompeting the effect of simultaneous POC production on the net metabolic balance. This hypothesis is difficult to test with field observations due to inclement fall and winter conditions. However, float observations now make it possible to confirm that seasonal DOC consumption occurs simultaneously with POC and PIC production and positive $F_{POC_{sinking}}$ during fall and winter (Figures 4b and 4c), aligning with the recent finding by Haskell et al. (2020) associated with the long-term climatology. This implies that DOC consumption can sustain the observed heterotrophy and the heterotrophic state does not equate to a lack of POC export. The observational evidence presented here lends insight to the ongoing debate regarding the metabolic state of the oligotrophic ocean, particularly in reconciling the prevalence of heterotrophy determined from incubation-based approaches with positive POC fluxes measured with ^{234}Th and sediment traps (Duarte et al., 2013; Williams et al., 2013).

The export ratio was typically low, with elevated values near the end of summer and two dominant peaks during December of 2018 and 2019 (Figures 5a and 5b). These winter periods were coincident with rapid deepening of the mixed layer (Figure 5c) suggesting that enhanced export efficiency was likely caused by the vertical redistribution of particles via seasonal physical mixing below the euphotic zone. Seasonal MLD shoaling can also lead to the detrainment of particles, referred to as the "mixed-layer pump". This process has been quantified in numerous regions through persistent, high-temporal-resolution observing with autonomous platforms (Boyd et al., 2019; Lacour et al., 2019; Llort et al., 2018; Xing et al., 2020). For example, by combining Argo float and satellite observations, Dall'Olmo et al. (2016) estimated that the mixed-layer pump may account for ~4% of carbon export globally, with larger contributions (up to 18%–30%) in high-latitude regions that experience dramatic seasonal MLD changes (Lacour et al., 2017, 2019). Recently, however, Xing et al. (2020) demonstrated that substantial underestimation of particle export can occur during winter in regions with sporadic mixed-layer pump events if floats are profiling as frequencies of 10, or even 5, days. This suggest that bio-optical approaches for quantifying carbon export from Argo floats operating on the normal 10-day profiling mission may not be accurate in some regions. In this study, we are able to robustly characterize carbon export potential by combining chemical and bio-optical sensor data, where chemical tracers convey the accumulated history and bio-optical tracers convey the in situ status of biological production in the upper layer.

3.3.2. Comparison of Float and Ship-Board Estimates of DOC Production

Seasonal removal and accumulation rates of DOC estimated from average ship-based euphotic zone DOC inventories (P24, P25, and P26) near the float trajectory (Figure 1) provide an independent constraint in the float DOC production estimate. Average DOC concentrations in the euphotic zone from ship observations varied between 50 to 75 μmol kg^{-1}, yielding an average removal rate of 3 ± 0.5 mmol C m^{-2} d^{-1} during fall/winter and accumulation rate of 5.5 ± 1.2 mmol C m^{-2} d^{-1} during spring/summer (Figure 6). This seasonal accumulation rate is comparable with prior estimates by Bif and Hansell (2019). If we assume that seasonal DOC accumulation and removal is primarily the result of biological (rather than physical) process, we find good agreement between float and ship estimates of DOC cycling (Figure 6b). There is a greater discrepancy between float and ship DOC production estimates during summer 2019, which is reflected in the C:N sensitivity analysis (Figure S4 in Supporting Information S1). DOC estimates during this period are very sensitive to the choice in $C:N_{POM}$ because the C:N ratio for TOM production is close to the end-member ratio of $C:N_{POM.}$ Thus, small uncertainties in $C:N_{POM}$ at this time can cause a large error in the computed DOC estimate. Future improvements could be made by considering temporal variability in end-member nutrient ratios.

3.3.3. Annual Integration

The 2019 annual export of POC derived from the euphotic zone DIC tracer budget (2.2 ± 0.2 mol C m^{-2} yr^{-1}) and the $F_{POC_{sinking}}$ term (2.2 ± 0.7 mol C m^{-2} yr^{-1}) are in excellent agreement (Figure 4d). This suggests that the majority of newly produced particles were exported out of the euphotic zone rather than respired or accumulated therein. The float-based estimates of POC flux are within the range of climatological values determined from a similar dual tracer budget approach (Haskell et al., 2020) and sediment trap observations (Timothy et al., 2013) from the same region.

Annual DOC production was 0.4 ± 0.3 mol C m^{-2} yr^{-1}, accounting for roughly 16 ± 8% of total organic matter production (Figure 4d). This falls at the lower range of prior studies in which DOC represented 20%–30% of the annual export production (Bif & Hansell, 2019; Emerson, 2014; Haskell et al., 2020). DOC estimates by Bif and

Hansell (2019) and Emerson (2014) were based on individual cruises or a single season and extrapolated to get an annual estimate, the former relying on an empirical relationship with spring and summer NO_3^- drawdown and the latter relying on May apparent unitization oxygen (AOU). The strong seasonality in DOC production presented in our study indicates the extrapolation from snapshot measurements to the annual cycle could be biased. By using a more sophisticated machining learning approach, coupled with biogeochemical models, to extrapolate discrete DOC production to the annual cycle, Roshan and DeVries (2017) obtained a ~15% contribution of DOC to total export in the high-latitude region of North Pacific, which is very close to our estimate.

Our study region is known to be a hot spot for $CaCO_3$ production where the contribution of PIC to annual carbon export can range from 18% to 30%, doubling the global average (Fassbender et al., 2016; Timothy et al., 2013). During our study period, PIC export was insignificant (0.12 ± 0.05 mol C m^{-2} yr^{-1}), contributing less than 5% to annual carbon export in 2019 (Figure 4d). *Emiliania huxleyi* is identified as the main calcifying species that drives PIC export in our study region (Putland et al., 2004). A prior study on phytoplankton community structure reported an increase in haptophytes (a gene mainly composed by *Emiliania huxleyi*) near our study region during a marine heatwave in 2013 (Peña et al., 2018). The cause of anomalously low PIC production in 2019 remains unclear.

4. Conclusions

Using all chemical and bio-optical sensors carried on a 5-sensor BGC float, we partitioned the export potential of distinct biogenic carbon pools; a process that has historically relied on snapshot ship-board observations. The float-based estimates revealed complex seasonal changes in each carbon pool and highlighted the need of continuous observations for more nuanced assessments of carbon cycling and export. Synchronicity between POC production and DOC consumption during fall and winter reflects key differences between the drivers of autotrophic and heterotrophic processes and sheds light on the mechanisms sustaining simultaneous particle export and heterotrophy in the Northeast Pacific. By combining float NPP estimates with in situ POC sinking flux estimates, we captured two high export ratio periods with different underlying mechanisms. While encouraging agreement in net DOC production estimated from float and ship-board observations suggests that our approach is reasonable and robust, it should be applied with care. Prior knowledge and constraint of local physical dynamics is essential, as a small and systematic error in each tracer budget will be propagated and amplified in the partitioning of carbon pools. Appropriate selection of the end-member nutrient ratios is equally important and challenging due to geographic variability and the sparsity of existing information.

A 5-sensor BGC float array is expanding throughout the global ocean through continued implementation of the Southern Ocean Carbon and Climate Observations and Modeling (SOMCOM) project, the Global Ocean Biogeochemistry (GO-BGC) Array, and other BGC Argo pilot arrays and projects. The multiple tracer approach proposed herein is scalable and could greatly improve understanding of the biological pump at regional and ultimately global scales. Satellite-based e-ratio algorithms have primarily been trained with datasets lacking DOC and/or PIC observations and that often do not capture seasonal and higher-frequency variations. Persistent and spatially distributed estimates of POC, DOC, and PIC production and export from the BGC float array would add substantial value by serving as the training data set for new satellite algorithms that capture all components of biogenic carbon cycling. Such nuanced information about biological productivity is critical for establishing baselines from which changes in ecosystem health and function can be assessed.

Conflict of Interest

The authors declare no conflicts of interest relevant to this study.

Data Availability Statement

All data required to conduct this study are publicly available through the links provided in the Methods section and tables in Supporting Information S1. This is PMEL Contribution No. 5280.

Acknowledgments
The authors are grateful to the Line P Program, sustained by the Institute of Ocean Sciences at the Department of Fisheries and Oceans, Canada, for decades of high-quality, curated observations made available to the public. The authors also thank the MBARI Chemical Sensor Group, led by Dr. Ken Johnson, and the UW Float Group, led by Dr. Steven Riser, for assistance with float deployment logistics, communications, and data quality control. The authors thank the captain and crew of the *R.V. Sally Ride* from which Dr. Scott Freeman and Dr. Mary Jane Perry deployed this float during the North Pacific NASA EXPORTS occupation. Y. Huang and this work were supported by an NSF grant to A. Fassbender (OCE1756932/OCE2032754). A. J. Fassbender, J. S. Long, and M. Bernardi Bif were supported by the David and Lucile Packard Foundation. A.J.F. received additional support from NOAA's Global Ocean Monitoring and Observing program. S.J. was supported by Fisheries and Oceans Canada.

References

Adkins, J. F., Naviaux, J. D., Subhas, A. V., Dong, S., & Berelson, W. M. (2021). The dissolution rate of $CaCO_3$ in the ocean. *Annual Review of Marine Science*, *13*, 57–80. https://doi.org/10.1146/annurev-marine-041720-092514

Alford, M. H., Cronin, M. F., & Klymak, J. M. (2012). Annual cycle and depth penetration of wind-generated near-inertial internal waves at Ocean Station Papa in the northeast Pacific. *Journal of Physical Oceanography*, *42*(6), 889–909. https://doi.org/10.1175/jpo-d-11-092.1

Alkire, M. B., D'Asaro, E., Lee, C., Jane Perry, M., Gray, A., Cetinić, I., et al. (2012). Estimates of net community production and export using high-resolution, Lagrangian measurements of O_2, NO_3^-, and POC through the evolution of a spring diatom bloom in the North Atlantic. *Deep Sea Research Part I: Oceanographic Research Papers*, *64*, 157–174. https://doi.org/10.1016/j.dsr.2012.01.012

Amaya, D. J., Miller, A. J., Xie, S. P., & Kosaka, Y. (2020). Physical drivers of the summer 2019 North Pacific marine heatwave. *Nature Communications*, *11*(1), 1903. https://doi.org/10.1038/s41467-020-15820-w

Amiel, D., Cochran, J. K., & Hirschberg, D. J. (2002). $^{234}Th/^{238}U$ disequilibrium as an indicator of the seasonal export flux of particulate organic carbon in the North Water. *Deep Sea Research Part II: Topical Studies in Oceanography*, *49*(22), 5191–5209. https://doi.org/10.1016/S0967-0645(02)00185-6

Anderson, L. A., & Sarmiento, J. L. (1994). Redfield ratios of remineralization determined by nutrient data analysis. *Global Biogeochemical Cycles*, *8*(1), 65–80. https://doi.org/10.1029/93gb03318

Ayers, J. M., & Lozier, M. S. (2012). Unraveling dynamical controls on the North Pacific carbon sink. *Journal of Geophysical Research: Oceans*, *117*(C1). https://doi.org/10.1029/2011jc007368

Balch, W., Drapeau, D., Bowler, B., & Booth, E. (2007). Prediction of pelagic calcification rates using satellite measurements. *Deep Sea Research Part II: Topical Studies in Oceanography*, *54*(5–7), 478–495. https://doi.org/10.1016/j.dsr2.2006.12.006

Behrenfeld, M. J., Boss, E., Siegel, D. A., & Shea, D. M. (2005). Carbon-based ocean productivity and phytoplankton physiology from space. *Global Biogeochemical Cycles*, *19*(1), GB1006. https://doi.org/10.1029/2004GB002299

Bender, M. L., Kinter, S., Cassar, N., & Wanninkhof, R. (2011). Evaluating gas transfer velocity parameterizations using upper ocean radon distributions. *Journal of Geophysical Research*, *116*(C2). https://doi.org/10.1029/2009jc005805

Bif, M. B., & Hansell, D. A. (2019). Seasonality of dissolved organic carbon in the upper Northeast Pacific Ocean. *Global Biogeochemical Cycles*, *33*, 526–539. https://doi.org/10.1029/2018gb006152

Bif, M. B., Siqueira, L., & Hansell, D. A. (2019). Warm events induce loss of resilience in organic carbon production in the Northeast Pacific Ocean. *Global Biogeochemical Cycles*, *33*(9), 1174–1186. https://doi.org/10.1029/2019gb006327

Bittig, H. C., Maurer, T. L., Plant, J. N., Schmechtig, C., Wong, A. P., Claustre, H., et al. (2019). A BGC-Argo guide: Planning, deployment, data handling and usage. *Frontiers in Marine Science*, *6*. https://doi.org/10.3389/fmars.2019.00502

Bittig, H. C., Steinhoff, T., Claustre, H., Fiedler, B., Williams, N. L., Sauzede, R., et al. (2018). An alternative to static climatologies: Robust estimation of open ocean CO_2 variables and nutrient concentrations from T, S, and O_2 data using Bayesian neural networks. *Frontiers in Marine Science*, *5*, 328. https://doi.org/10.3389/fmars.2018.00328

Bond, N. A., Cronin, M. F., Freeland, H., & Mantua, N. (2015). Causes and impacts of the 2014 warm anomaly in the NE Pacific. *Geophysical Research Letters*, *42*(9), 3414–3420. https://doi.org/10.1002/2015gl063306

Boudreau, B. P., Middelburg, J. J., & Luo, Y. (2018). The role of calcification in carbonate compensation. *Nature Geoscience*, *11*(12), 894–900. https://doi.org/10.1038/s41561-018-0259-5

Boyd, P. W., Claustre, H., Levy, M., Siegel, D. A., & Weber, T. (2019). Multi-faceted particle pumps drive carbon sequestration in the ocean. *Nature*, *568*(7752), 327–335. https://doi.org/10.1038/s41586-019-1098-2

Brewer, P. G., & Goldman, J. C. (1976). Alkalinity changes generated by phytoplankton growth. *Limnology and Oceanography*, *21*(1), 108–117. https://doi.org/10.4319/lo.1976.21.1.0108

Briggs, N., Dall'Olmo, G., & Claustre, H. (2020). Major role of particle fragmentation in regulating biological sequestration of CO_2 by the oceans. *Science*, *367*(6479), 791–793. https://doi.org/10.1126/science.aay1790

Buesseler, K. O. (1991). Do upper-ocean sediment traps provide an accurate record of particle flux? *Nature*, *353*(6343), 420–423. https://doi.org/10.1038/353420a0

Buesseler, K. O., Boyd, P. W., Black, E. E., & Siegel, D. A. (2020). Metrics that matter for assessing the ocean biological carbon pump. *Proceedings of the National Academy of Sciences*, *117*(18), 9679–9687. https://doi.org/10.1073/pnas.1918114117

Bushinsky, S. M., & Emerson, S. (2015). Marine biological production from in situ oxygen measurements on a profiling float in the subarctic Pacific Ocean. *Global Biogeochemical Cycles*, *29*(12), 2050–2060. https://doi.org/10.1002/2015gb005251

Bushinsky, S. M., Emerson, S. R., Riser, S. C., & Swift, D. D. (2016). Accurate oxygen measurements on modified Argo floats using in situ air calibrations. *Limnology and Oceanography: Methods*, *14*(8), 491–505. https://doi.org/10.1002/lom3.10107

Carlson, C. A., Ducklow, H. W., & Michaels, A. F. (1994). Annual flux of dissolved organic carbon from the euphotic zone in the northwestern Sargasso Sea. *Nature*, *371*(371), 405–408. https://doi.org/10.1038/371405a0

Carlson, C. A., Hansell, D. A., Nelson, N. B., Siegel, D. A., Smethie, W. M., Khatiwala, S., et al. (2010). Dissolved organic carbon export and subsequent remineralization in the mesopelagic and bathypelagic realms of the North Atlantic basin. *Deep Sea Research Part II: Topical Studies in Oceanography*, *57*(16), 1433–1445. https://doi.org/10.1016/j.dsr2.2010.02.013

Carter, B. R., Feely, R. A., Lauvset, S. K., Olsen, A., DeVries, T., Sonnerup, R., et al. (2021). Preformed properties for marine organic matter and carbonate mineral cycling quantification. *Global Biogeochemical Cycles*, *35*, e2020GB006623. https://doi.org/10.1029/2020gb006623

Cavan, E. L., Henson, S. A., Belcher, A., & Sanders, R. (2017). Role of zooplankton in determining the efficiency of the biological carbon pump. *Biogeosciences*, *14*(1), 177–186. https://doi.org/10.5194/bg-14-177-2017

Chou, W. C., Sheu, D. D., Chen, C. T. A., Wang, S. L., & Tseng, C. M. (2005). Seasonal variability of carbon chemistry at the SEATS time-series site, northern South China Sea between 2002 and 2003. *Terrestrial, Atmospheric and Oceanic Sciences*, *16*(2), 445–465. https://doi.org/10.3319/tao.2005.16.2.445(o)

Coale, K. H., & Bruland, K. W. (1985). $^{234}Th:^{238}U$ disequilibria within the California Current. *Limnology and Oceanography*, *30*(1), 22–33. https://doi.org/10.4319/lo.1985.30.1.0022

Cronin, M. F., Pelland, N. A., Emerson, S. R., & Crawford, W. R. (2015). Estimating diffusivity from the mixed layer heat and salt balances in the North Pacific. *Journal of Geophysical Research: Oceans*, *120*(11), 7346–7362. https://doi.org/10.1002/2015jc011010

Dall'Olmo, G., Dingle, J., Polimene, L., Brewin, R. J. W., & Claustre, H. (2016). Substantial energy input to the mesopelagic ecosystem from the seasonal mixed-layer pump. *Nature Geoscience*, *9*(11), 820–823. https://doi.org/10.1038/ngeo2818

de Boyer Montégut, C., Madec, G., Fischer, A. S., Lazar, A., & Iudicone, D. (2004). Mixed layer depth over the global ocean: An examination of profile data and a profile-based climatology. *Journal of Geophysical Research: Oceans*, *109*, C12003. https://doi.org/10.1029/2004JC002378

Deutsch, C., Gruber, N., Key, R. M., Sarmiento, J. L., & Ganachaud, A. (2001). Denitrification and N_2 fixation in the Pacific Ocean. *Global Biogeochemical Cycles*, *15*(2), 483–506. https://doi.org/10.1029/2000gb001291

DeVries, T., & Weber, T. (2017). The export and fate of organic matter in the ocean: New constraints from combining satellite and oceanographic tracer observations. *Global Biogeochemical Cycles*, *31*(3), 535–555. https://doi.org/10.1002/2016gb005551

Duarte, C. M., Regaudie-de-Gioux, A., Arrieta, J. M., Delgado-Huertas, A., & Agusti, S. (2013). The oligotrophic ocean is heterotrophic. *Annual Review of Marine Science*, *4*, 551–569. https://doi.org/10.1146/annurev-marine-121211-172337

Dunne, J. P., Sarmiento, J. L., & Gnanadesikan, A. (2007). A synthesis of global particle export from the surface ocean and cycling through the ocean interior and on the seafloor. *Global Biogeochemical Cycles*, *21*(4), GB4006. https://doi.org/10.1029/2006gb002907

Emerson, S. (2014). Annual net community production and the biological carbon flux in the ocean. *Global Biogeochemical Cycles*, *28*(1), 14–28. https://doi.org/10.1002/2013gb004680

Emerson, S., & Stump, C. (2010). Net biological oxygen production in the ocean—II: Remote in situ measurements of O_2 and N_2 in subarctic pacific surface waters. *Deep Sea Research Part I: Oceanographic Research Papers*, *57*(10), 1255–1265. https://doi.org/10.1016/j.dsr.2010.06.001

Emerson, S., Yang, B., White, M., & Cronin, M. (2019). Air-sea gas transfer: Determining bubble fluxes with in situ N_2 observations. *Journal of Geophysical Research: Oceans*, *124*(4), 2716–2727. https://doi.org/10.1029/2018jc014786

Fassbender, A. J., Sabine, C. L., & Cronin, M. F. (2016). Net community production and calcification from seven years of NOAA Station Papa Mooring measurements. *Global Biogeochemical Cycles*, *30*(2), 250–267. https://doi.org/10.1002/2015GB005205

Fassbender, A. J., Sabine, C. L., Cronin, M. F., & Sutton, A. J. (2017). Mixed-layer carbon cycling at the Kuroshio Extension Observatory. *Global Biogeochemical Cycles*, *31*, 272–288. https://doi.org/10.1002/2016gb005547

Feely, R. A., Sabine, C. L., Lee, K., Berelson, W., Kleypas, J., Millero, F. J., et al. (2004). Impact of anthropogenic CO_2 on the $CaCO_3$ system in the oceans. *Science*, *305*(5682), 362–366. https://doi.org/10.1126/science.1097329

Freeland, H. (2007). A short history of Ocean Station Papa and Line P. *Progress in Oceanography*, *75*(2), 120–125. https://doi.org/10.1016/j.pocean.2007.08.005

Friedlingstein, P., O'Sullivan, M., Jones, M. W., Andrew, R. M., Hauck, J., et al. (2020). Global carbon budget 2020. *Earth System Science Data*, *12*(4), 3269–3340. https://doi.org/10.5194/essd-12-3269-2020

Garcia, H. E., & Gordon, L. I. (1992). Oxygen solubility in seawater-better fitting equations. *Limnology and Oceanography*, *37*(6), 1307–1312. https://doi.org/10.4319/lo.1992.37.6.1307

Gattuso, P., Epitalon, M., Lavigne, H., & Orr, J. (2020). *Seacarb: Seawater carbonate chemistry. R package version 3.2.13*. Retrieved from http://CRAN.R-project.org/package=seacarb

Giesbrecht, K. E., Hamme, R. C., & Emerson, S. R. (2012). Biological productivity along Line P in the subarctic northeast Pacific: In situ versus incubation-based methods. *Global Biogeochemical Cycles*, *26*(3). https://doi.org/10.1029/2012gb004349

Goldblatt, R. H., Mackas, D. L., & Lewis, A. G. (1999). Mesozooplankton community characteristics in the NE subarctic Pacific. *Deep Sea Research Part II: Topical Studies in Oceanography*, *46*(11–12), 2619–2644. https://doi.org/10.1016/s0967-0645(99)00078-8

Graff, J. R., Westberry, T. K., Milligan, A. J., Brown, M. B., Dall'Olmo, G., van Dongen-Vogels, V., et al. (2015). Analytical phytoplankton carbon measurements spanning diverse ecosystems. *Deep Sea Research Part I: Oceanographic Research Papers*, *102*, 16–25. https://doi.org/10.1016/j.dsr.2015.04.006

Haentjens, N., Della Penna, A., Briggs, N., Karp-Boss, L., Gaube, P., Boss, E., et al. (2020). Detecting mesopelagic organisms using biogeochemical-Argo floats. *Geophysical Research Letters*, *47*(6), e2019GL086088. https://doi.org/10.1029/2019GL086088

Hansell, D. A., & Carlson, C. A. (1998). Net community production of dissolved organic carbon. *Global Biogeochemical Cycles*, *12*(3), 443–453. https://doi.org/10.1029/98GB01928

Hansell, D. A., Carlson, C. A., Repeta, D. J., & Schlitzer, R. (2009). Dissolved organic matter in the ocean: A controversy stimulates new insights. *Oceanography*, *22*(4), 202–211. https://doi.org/10.5670/oceanog.2009.109

Harrison, P. J. (2002). Station Papa time series: Insights into ecosystem dynamics. *Journal of Oceanography*, *58*(2), 259–264. https://doi.org/10.1023/a:1015857624562

Haskell, W. Z., Fassbender, A. J., Long, J. S., & Plant, J. N. (2020). Annual net community production of particulate and dissolved organic carbon from a decade of biogeochemical profiling float observations in the Northeast Pacific. *Global Biogeochemical Cycles*, *34*(10). https://doi.org/10.1029/2020gb006599

Henson, S. A., Sanders, R., Madsen, E., Morris, P. J., Le Moigne, F., Quartly, G. D., et al. (2011). A reduced estimate of the strength of the ocean's biological carbon pump. *Geophysical Research Letters*, *38*(4), L04606. https://doi.org/10.1029/2011gl046735

Hygum, B. H., Petersen, J. W., & Søndergaard, M. (1997). Dissolved organic carbon released by zooplankton grazing activity–A high-quality substrate pool for bacteria. *Journal of Plankton Research*, *19*(1), 97–111. https://doi.org/10.1093/plankt/19.1.97

Johnson, K. S., & Coletti, L. J. (2002). In situ ultraviolet spectrophotometry for high resolution and long-term monitoring of nitrate, bromide and bisulfide in the ocean. *Deep Sea Research Part I: Oceanographic Research Papers*, *49*(7), 1291–1305. https://doi.org/10.1016/s0967-0637(02)00020-1

Johnson, K. S., Jannasch, H. W., Coletti, L. J., Elrod, V. A., Martz, T. R., Takeshita, Y., et al. (2016). Deep-Sea DuraFET: A pressure tolerant pH sensor designed for global sensor networks. *Analytical Chemistry*, *88*(6), 3249–3256. https://doi.org/10.1021/acs.analchem.5b04653

Johnson, K. S., Plant, J. N., Coletti, L. J., Jannasch, H. W., Sakamoto, C. M., Riser, S. C., et al. (2017). Biogeochemical sensor performance in the SOCCOM profiling float array. *Journal of Geophysical Research: Oceans*, *122*(8), 6416–6436. https://doi.org/10.1002/2017jc012838

Klaas, C., & Archer, D. E. (2002). Association of sinking organic matter with various types of mineral ballast in the deep sea: Implications for the rain ratio. *Global Biogeochemical Cycles*, *16*(4), 1116. https://doi.org/10.1029/2001gb001765

Körtzinger, A., Send, U., Lampitt, R. S., Hartman, S., Wallace, D. W. R., Karstensen, J., et al. (2008). The seasonal pCO_2 cycle at 49°N/16.5°W in the northeastern Atlantic Ocean and what it tells us about biological productivity. *Journal of Geophysical Research*, *113*(C4). https://doi.org/10.1029/2007jc004347

Kwon, E. Y., Primeau, F., & Sarmiento, J. L. (2009). The impact of remineralization depth on the air–sea carbon balance. *Nature Geoscience*, *2*(9), 630–635. https://doi.org/10.1038/ngeo612

Lacour, L., Ardyna, M., Stec, K. F., Claustre, H., Prieur, L., Poteau, A., et al. (2017). Unexpected winter phytoplankton blooms in the North Atlantic subpolar gyre. *Nature Geoscience*, *10*(11), 836–839. https://doi.org/10.1038/ngeo3035

Lacour, L., Briggs, N., Claustre, H., Ardyna, M., & Dall'Olmo, G. (2019). The intraseasonal dynamics of the mixed layer pump in the subpolar North Atlantic Ocean: A Biogeochemical-Argo float approach. *Global Biogeochemical Cycles*, *33*(3), 266–281. https://doi.org/10.1029/2018gb005997

Lampert, W. (1978). Release of dissolved organic carbon by grazing zooplankton. *Limnology and Oceanography*, *23*(4), 831–834. https://doi.org/10.4319/lo.1978.23.4.0831

Landry, M. R., Monger, B. C., & Selph, K. E. (1993). Time-dependency of microzooplankton grazing and phytoplankton growth in the subarctic Pacific. *Progress in Oceanography*, *32*(1–4), 205–222. https://doi.org/10.1016/0079-6611(93)90014-5

Laws, E. A., D'Sa, E., & Naik, P. (2011). Simple equations to estimate ratios of new or export production to total production from satellite-derived estimates of sea surface temperature and primary production. *Limnology and Oceanography: Methods*, *9*(12), 593–601. https://doi.org/10.4319/lom.2011.9.593

Legendre, L., Rivkin, R. B., Weinbauer, M. G., Guidi, L., & Uitz, J. (2015). The microbial carbon pump concept: Potential biogeochemical significance in the globally changing ocean. *Progress in Oceanography*, *134*, 432–450. https://doi.org/10.1016/j.pocean.2015.01.008

Liang, J.-H., Deutsch, C., McWilliams, J. C., Baschek, B., Sullivan, P. P., & Chiba, D. (2013). Parameterizing bubble-mediated air-sea gas exchange and its effect on ocean ventilation. *Global Biogeochemical Cycles*, *27*(3), 894–905. https://doi.org/10.1002/gbc.20080

Llort, J., Langlais, C., Matear, R., Moreau, S., Lenton, A., & Strutton, P. G. (2018). Evaluating Southern Ocean carbon eddy-pump from biogeochemical-Argo floats. *Journal of Geophysical Research: Oceans*, *123*(2), 971–984. https://doi.org/10.1002/2017jc012861

Long, J. S., Fassbender, A. J., & Estapa, M. L. (2021). Depth-resolved net primary production in the Northeast Pacific Ocean: A comparison of satellite and profiling float estimates in the context of two marine heatwaves. *Geophysical Research Letters*, *48*(19). https://doi.org/10.1029/2021gl093462

Ma, L., Xiao, W., Laws, E. A., Bai, X., Chiang, K. P., Liu, X., et al. (2020). Responses of phytoplankton communities to the effect of internal wave-powered upwelling. *Limnology and Oceanography*, *66*(4), 1083–1098. https://doi.org/10.1002/lno.11666

Macreadie, P. I., Serrano, O., Maher, D. T., Duarte, C. M., & Beardall, J. (2017). Addressing calcium carbonate cycling in blue carbon accounting. *Limnology and Oceanography Letters*, *2*(6), 195–201. https://doi.org/10.1002/lol2.10052

Martin, J. H., & Fitzwater, S. E. (1988). Iron deficiency limits phytoplankton growth in the north-east Pacific subarctic. *Nature*, *331*(6154), 341–343. https://doi.org/10.1038/331341a0

Martin, J. H., Knauer, G. A., Karl, D. M., & Broenkow, W. W. (1987). VERTEX: Carbon cycling in the northeast Pacific. *Deep-Sea Research*, *34*(2), 267–285. https://doi.org/10.1016/0198-0149(87)90086-0

Maurer, T. L., Plant, J. N., & Johnson, K. S. (2021). Delayed-mode quality control of oxygen, nitrate, and pH data on SOCCOM biogeochemical profiling floats. *Frontiers in Marine Science*, *8*. https://doi.org/10.3389/fmars.2021.683207

Myklestad, S. M. (2000). Dissolved organic carbon from phytoplankton. In *Marine chemistry* (pp. 111–148). Springer.

Nielsen, J. M., Rogers, L. A., Brodeur, R. D., Thompson, A. R., Auth, T. D., Deary, A. L., et al. (2021). Responses of ichthyoplankton assemblages to the recent marine heatwave and previous climate fluctuations in several Northeast Pacific marine ecosystems. *Global Change Biology*, *27*(3), 506–520. https://doi.org/10.1111/gcb.15415

Palevsky, H. I., & Doney, S. C. (2018). How choice of depth horizon influences the estimated spatial patterns and global magnitude of ocean carbon export flux. *Geophysical Research Letters*, *45*(9), 4171–4179. https://doi.org/10.1029/2017gl076498

Passow, U. (2002). Transparent exopolymer particles (TEP) in aquatic environments. *Progress in Oceanography*, *55*(3–4), 287–333. https://doi.org/10.1016/s0079-6611(02)00138-6

Passow, U., & Carlson, C. A. (2012). The biological pump in a high CO_2 world. *Marine Ecology Progress Series*, *470*, 249–271. https://doi.org/10.3354/meps09985

Pelland, N. A., Eriksen, C. C., Emerson, S. R., & Cronin, M. F. (2018). Seaglider surveys at Ocean Station Papa: Oxygen kinematics and upper-ocean metabolism. *Journal of Geophysical Research: Oceans*, *123*(9), 6408–6427. https://doi.org/10.1029/2018jc014091

Peña, M. A., Nemcek, N., & Robert, M. (2018). Phytoplankton responses to the 2014–2016 warming anomaly in the northeast subarctic Pacific Ocean. *Limnology and Oceanography*, *64*(2), 515–525. https://doi.org/10.1002/lno.11056

Plant, J. N., Johnson, K. S., Sakamoto, C. M., Jannasch, H. W., Coletti, L. J., Riser, S. C., & Swift, L. J. (2016). Net community production at Ocean Station Papa observed with nitrate and oxygen sensors on profiling floats. *Global Biogeochemical Cycles*, *30*(6), 859–879. https://doi.org/10.1002/2015gb005349

Putland, J. N., Whitney, F. A., & Crawford, D. W. (2004). Survey of bottom-up controls of *Emiliania huxleyi* in the Northeast Subarctic Pacific. *Deep Sea Research Part I: Oceanographic Research Papers*, *51*(12), 1793–1802. https://doi.org/10.1016/j.dsr.2004.08.001

Quay, P., & Stutsman, J. (2003). Surface layer carbon budget for the subtropical N. Pacific: Constraints at station ALOHA. *Deep Sea Research Part I: Oceanographic Research Papers*, *50*(9), 1045–1061. https://doi.org/10.1016/s0967-0637(03)00116-x

Regaudie-de-Gioux, A., Lasternas, S. b., Agustí, S., & Duarte, C. M. (2014). Comparing marine primary production estimates through different methods and development of conversion equations. *Frontiers in Marine Science*, *1*, 19. https://doi.org/10.3389/fmars.2014.00019

Riser, S. C., & Johnson, K. S. (2008). Net production of oxygen in the subtropical ocean. *Nature*, *451*(7176), 323–325. https://doi.org/10.1038/nature06441

Roemmich, D., Alford, M. H., Claustre, H., Johnson, K., King, B., Moum, J., et al. (2019). On the future of Argo: A global, full-depth, multi-disciplinary array. *Frontiers in Marine Science*, *6*. https://doi.org/10.3389/fmars.2019.00439

Romera-Castillo, C., Letscher, R. T., & Hansell, D. A. (2016). New nutrients exert fundamental control on dissolved organic carbon accumulation in the surface Atlantic Ocean. *Proceedings of the National Academy of Sciences*, *113*(38), 10497–10502. https://doi.org/10.1073/pnas.1605344113

Roshan, S., & DeVries, T. (2017). Efficient dissolved organic carbon production and export in the oligotrophic ocean. *Nature Communications*, *8*(1), 2036. https://doi.org/10.1038/s41467-017-02227-3

Sabine, C. L., & Tanhua, T. (2010). Estimation of anthropogenic CO_2 inventories in the ocean. *Annual Review of Marine Science*, *2*, 175–198. https://doi.org/10.1146/annurev-marine-120308-080947

Scannell, H. A., Johnson, G. C., Thompson, L., Lyman, J. M., & Riser, S. C. (2020). Subsurface evolution and persistence of marine heatwaves in the Northeast Pacific. *Geophysical Research Letters*, *47*(23). https://doi.org/10.1029/2020gl090548

Sherry, N. D., Boyd, P. W., Sugimoto, K., & Harrison, P. J. (1999). Seasonal and spatial patterns of heterotrophic bacterial production, respiration, and biomass in the subarctic NE Pacific. *Deep Sea Research Part II: Topical Studies in Oceanography*, *46*(11), 2557–2578. https://doi.org/10.1016/S0967-0645(99)00076-4

Sherry, N. D., Imanian, B., Sugimoto, K., Boyd, P. W., & Harrison, P. J. (2002). Seasonal and interannual trends in heterotrophic bacterial processes between 1995 and 1999 in the subarctic NE Pacific. *Deep Sea Research Part II: Topical Studies in Oceanography*, *49*(24), 5775–5791. https://doi.org/10.1016/S0967-0645(02)00214-X

Shroyer, E., Rudnick, D., Farrar, J. T., Lim, B., Venayagamoorthy, S. K., St. Laurent, L. C., et al. (2016). Modification of upper-ocean temperature structure by subsurface mixing in the presence of strong salinity stratification. *Oceanography*, *29*(2), 62–71. https://doi.org/10.5670/oceanog.2016.39

Siegel, D. A., Buesseler, K. O., Doney, S. C., Sailley, S. F., Behrenfeld, M. J., & Boyd, P. W. (2014). Global assessment of ocean carbon export by combining satellite observations and food-web models. *Global Biogeochemical Cycles*, *28*(3), 181–196. https://doi.org/10.1002/2013GB004743

Signorini, S. R., McClain, C. R., Christian, J. R., & Wong, C. S. (2001). Seasonal and interannual variability of phytoplankton, nutrients, TCO_2, pCO_2, and O_2 in the eastern subarctic Pacific (ocean weather station Papa). *Journal of Geophysical Research: Oceans*, *106*(C12), 31197–31215. https://doi.org/10.1029/2000jc000343

Sulpis, O., Jeansson, E., Dinauer, A., Lauvset, S. K., & Middelburg, J. J. (2021). Calcium carbonate dissolution patterns in the ocean. *Nature Geoscience*. https://doi.org/10.1038/s41561-021-00743-y

Sun, O. M., Jayne, S. R., Polzin, K. L., Rahter, B. A., & St. Laurent, L. C. (2013). Scaling turbulent dissipation in the transition layer. *Journal of Physical Oceanography*, *43*(11), 2475–2489. https://doi.org/10.1175/jpo-d-13-057.1

Takahashi, T., Sutherland, S. C., Sweeney, C., Poisson, A., Metzl, N., Tilbrook, B., et al. (2002). Global sea–air CO_2 flux based on climatological surface ocean pCO_2, and seasonal biological and temperature effects. *Deep Sea Research Part II: Topical Studies in Oceanography*, *49*(9–10), 1601–1622. https://doi.org/10.1016/s0967-0645(02)00003-6

Takeshita, Y., Martz, T. R., Johnson, K. S., Plant, J. N., Gilbert, D., Riser, S. C., et al. (2013). A climatology-based quality control procedure for profiling float oxygen data. *Journal of Geophysical Research: Oceans*, *118*(10), 5640–5650. https://doi.org/10.1002/jgrc.20399

Tang, W., Li, Z., & Cassar, N. (2019). Machine learning estimates of global marine nitrogen fixation. *Journal of Geophysical Research: Biogeosciences*, *124*(3), 717–730. https://doi.org/10.1029/2018jg004828

Teira, E., José Pazó, M., Serret, P., & Fernández, E. (2001). Dissolved organic carbon production by microbial populations in the Atlantic Ocean. *Limnology and Oceanography*, *46*(6), 1370–1377. https://doi.org/10.4319/lo.2001.46.6.1370

Timothy, D. A., Wong, C. S., Barwell-Clarke, J. E., Page, J. S., White, L. A., Macdonald, R. W., et al. (2013). Climatology of sediment flux and composition in the subarctic Northeast Pacific Ocean with biogeochemical implications. *Progress in Oceanography*, *116*, 95–129. https://doi.org/10.1016/j.pocean.2013.06.017

Tyrrell, T., & Lucas, M. I. (2002). Geochemical evidence of denitrification in the Benguela upwelling system. *Continental Shelf Research*, *22*(17), 2497–2511. https://doi.org/10.1016/s0278-4343(02)00077-8

Volk, T., & Hoffert, M. I. (1985). Ocean carbon pumps: Analysis of relative strengths and efficiencies in ocean-driven atmospheric CO_2 changes. *The carbon cycle and atmospheric CO_2: Natural variations Archean to present*. https://doi.org/10.1029/GM032p0099

Wang, W. L., Moore, J. K., Martiny, A. C., & Primeau, F. W. (2019). Convergent estimates of marine nitrogen fixation. *Nature*, *566*(7743), 205–211. https://doi.org/10.1038/s41586-019-0911-2

Wanninkhof, R. (2014). Relationship between wind speed and gas exchange over the ocean revisited. *Limnology and Oceanography: Methods*, *12*(6), 351–362. https://doi.org/10.4319/lom.2014.12.351

Weiss, R. F. (1974). Carbon dioxide in water and seawater: The solubility of a non-ideal gas. *Marine Chemistry*, *2*(3), 203–215. https://doi.org/10.1016/0304-4203(74)90015-2

Westberry, T., Behrenfeld, M. J., Siegel, D. A., & Boss, E. (2008). Carbon-based primary productivity modeling with vertically resolved photoacclimation. *Global Biogeochemical Cycles*, *22*(2). https://doi.org/10.1029/2007gb003078

Williams, N. L., Juranek, L. W., Feely, R. A., Russell, J. L., Johnson, K. S., & Hales, B. (2018). Assessment of the carbonate chemistry seasonal cycles in the Southern Ocean from persistent observational platforms. *Journal of Geophysical Research: Oceans*, *123*(7), 4833–4852. https://doi.org/10.1029/2017jc012917

Williams, P. J. L. B., Quay, P. D., Westberry, T. K., & Behrenfeld, M. J. (2013). The oligotrophic ocean is autotrophic. *Annual Review of Marine Science*, *5*(1), 535–549. https://doi.org/10.1146/annurev-marine-121211-172335

Wong, C. S., Waser, N. A. D., Whitney, F. A., Johnson, W. K., & Page, J. S. (2002). Time-series study of the biogeochemistry of the North East subarctic Pacific: Reconciliation of the C_{org}/N remineralization and uptake ratios with the Redfield ratios. *Deep Sea Research Part II: Topical Studies in Oceanography*, *49*(24–25), 5717–5738. https://doi.org/10.1016/s0967-0645(02)00211-4

Wong, C. S., Whitney, F. A., Crawford, D. W., Iseki, K., Matear, R. J., Johnson, W. K., et al. (1999). Seasonal and interannual variability in particle fluxes of carbon, nitrogen and silicon from time series of sediment traps at Ocean Station P, 1982–1993: Relationship to changes in subarctic primary productivity. *Deep Sea Research Part II: Topical Studies in Oceanography*, *46*(11–12), 2735–2760. https://doi.org/10.1016/s0967-0645(99)00082-x

Xing, X., Wells, M. L., Chen, S., Lin, S., & Chai, F. (2020). Enhanced winter carbon export observed by BGC-Argo in the Northwest Pacific Ocean. *Geophysical Research Letters*, *47*(22). https://doi.org/10.1029/2020gl089847

Yang, B., Emerson, S. R., & Bushinsky, S. M. (2017). Annual net community production in the subtropical Pacific Ocean from in situ oxygen measurements on profiling floats. *Global Biogeochemical Cycles*, *31*, 728–744. https://doi.org/10.1002/2016GB005545

Yang, B., Emerson, S. R., & Peña, M. A. (2018). The effect of the 2013–2016 high temperature anomaly in the subarctic Northeast Pacific (the "Blob") on net community production. *Biogeosciences*, *15*(21), 6747–6759. https://doi.org/10.5194/bg-15-6747-2018